Marine and Petroleum Geology 68 (2015) 629–647

Contents lists available at ScienceDirect

Marine and Petroleum Geology

journal homepage: www.elsevier.com/locate/marpetgeo

Research paper

Seismic characterization of a Bottom Simulating Reflection (BSR) and plumbing system of the Cameroon margin, offshore West Africa

Anh Ngoc Le*, Mads Huuse, Jonathan Redfern, Rob L. Gawthorpe, Duncan Irving

University of Manchester, School of Earth, Atmospheric and Environmental Sciences, Williamson Building, Oxford Road, Manchester M13 9PL, UK

ARTICLE INFO

Article history:
Received 16 January 2014
Received in revised form
6 December 2014
Accepted 10 December 2014
Available online 18 December 2014

Keywords:
Bottom Simulating Reflection (BSR)
Gas hydrate
Pockmark
Fluid migration
Gas chimney

ABSTRACT

Analysis of a high-resolution 3D seismic dataset covering part of the Cameroon continental margin reveals a previously undocumented gas hydrate related Bottom Simulating Reflection (BSR) in water depths ranging from 940 m–1750 m. The BSR is mapped over an area of 350 km^2, and at sub-sea depth of 104 m –250 m, increasing with increasing water depth. It is observed to vary in character depending on the present-day seabed slope gradient. In areas of low slope gradient, the BSR is high amplitude, with high amplitude reflections below it, and is associated with gas chimneys and single pockmarks. The high amplitude reflections immediately beneath the BSR are interpreted to indicate the presence of free gas, trapped under the hydrate seal and within thin sands within the sub-BSR free gas zone. In areas of high gradient slope, the BSR is comparatively weak and is associated with pockmark trains and pockmark clusters. The weakness of the BSR is interpreted to be caused by a lack of trapped free gas and thus low velocity contrast.

The observed seabed pockmarks have been classified into three types defined by their appearance and distribution: (1) single pockmarks, (2) pockmark trains, and (3) pockmark clusters. Each style of pockmarks is related to a particular type of fluid migration pathway. The results suggest a number of migration mechanisms that deliver gas to the shallow succession, largely sealed beneath the gas hydrate, but also reaching the sea floor locally as evidenced by the pockmarks. The origin of the gas cannot be ascertained with the present data, but the style of overburden leakage features documented here is commonly found in petroleum provinces.

1. Introduction

Bottom Simulating Reflections (BSRs) are seismic reflections that parallel the seafloor, cross-cutting primary stratal reflections where these are oblique to the seafloor. BSRs are generally related to diagenetic processes such as opal A to CT transformation or fluid migration and storage in the shallow subsurface (Berndt et al., 2004). They are controlled by the temperature and pressure within the shallow subsurface (Kvenvolden and Barnard, 1982; Sloan, 2003). The BSRs caused by the presence of gas hydrate and underlying free gas 'simulate' the sea bed surface by following the sea floor topography as they essentially follow the temperature (isotherm) and pressure conditions, which are mainly controlled by depth of burial (Dillon et al., 1994).

This study documents the existence of a gas hydrate-related BSR in deep water offshore Cameroon. Methane hydrates are formed at appropriate temperature and pressure conditions when water is saturated with methane and freezes to form the cubic clathrate structure ($CH_4 \cdot 7H_2O$) in which gas molecules are trapped in the voids within the crystal lattice (Sloan, 2003). The existence of hydrate reduces the rock permeability considerably, creating layers that act as a seal trapping free gas within the more permeable hydrate free sediments below (Dillon et al., 1994). The thickness of the GHSZ is mainly determined by water depth (as it controls ambient pressure), bottom-water temperature and geothermal gradient, and as a general rule, the greater the water depth the thicker the potential gas hydrate-bearing interval (Kvenvolden and Barnard, 1982). The BSR therefore roughly parallels the seafloor and increases in depth as a function of water depth with local modulations caused by variations in geotherm, presence of fluid advection, sediment physical and thermal properties, and recent erosional events (Hornbach et al., 2008); where the seafloor is very

* Corresponding author. Petroleum Geology Department, Hanoi University of Mining and Geology, Dong Ngac, Tu Liem, Hanoi, Viet Nam.
E-mail address: anh77anh@yahoo.com (A.N. Le).

http://dx.doi.org/10.1016/j.marpetgeo.2014.12.006
0264-8172/

irregular, the BSR underneath is commonly smoother due to thermal diffusion in the subsurface. Gas hydrate-related BSRs have been documented along both passive and active margins where water depths exceed 300 m (Kvenvolden et al., 1993; Cunningham and Lindholm, 2000). Gas hydrate-related BSRs can be recognised based on five key criteria: (1) A change in seismic reflection polarity (opposite to the sea floor reflection); (2) Presence of a reflection cross-cutting primary stratal reflections. However, when the angle of cross-cutting is small, the polarity of the cross-cutting event is difficult to determine due to the interference of reflections (Berndt et al., 2004; Calvès et al., 2008); (3) Locations at specific depth range (pressure) and temperature that define a clathrate–water equilibrium curve (Dickens and Quinby-Hunt, 1997; Sloan, 2003); (4) Changes in seismic character, with common amplitude blanking/reduction above the BSR compared with the reflection amplitudes below; (5) Presence of bright seismic anomalies caused by the presence of free gas below the BSR.

In this study, we have observed many of the above characteristics, and some additional features, including in particular some high amplitude reflections observed at a maximum of 80 ms TWT above the BSR in the 'blanking' zone. This paper utilizes a high quality 3D seismic dataset to document the nature of a newly discovered BSR in a deepwater slope area offshore southern Cameroon and describes how the BSR occurrences are related to slope geomorphology, fluid-related features and stratigraphic variations within the slope sequence. We then discuss the possible controls on fluid storage, migration and BSR occurrence.

2. Geological setting

The study covers an area of approximately 1500 km^2 of the Kribi-Campo sub-basin, between 2°20′ N to 3°00′N latitude, 9°00 E to 9°50′ E longitude (Fig. 1), corresponding to the southern part of Douala basin, offshore Cameroon. The basin is limited to the south by the Campo high, which separates the Kribi-Campo sub-basin from the Equatorial Guinea basin. The northern limit of the basin is difficult to define. It may correspond to the northern limit of the Aptian salt deposits. The onshore part of the Kribi-Campo sub-basin

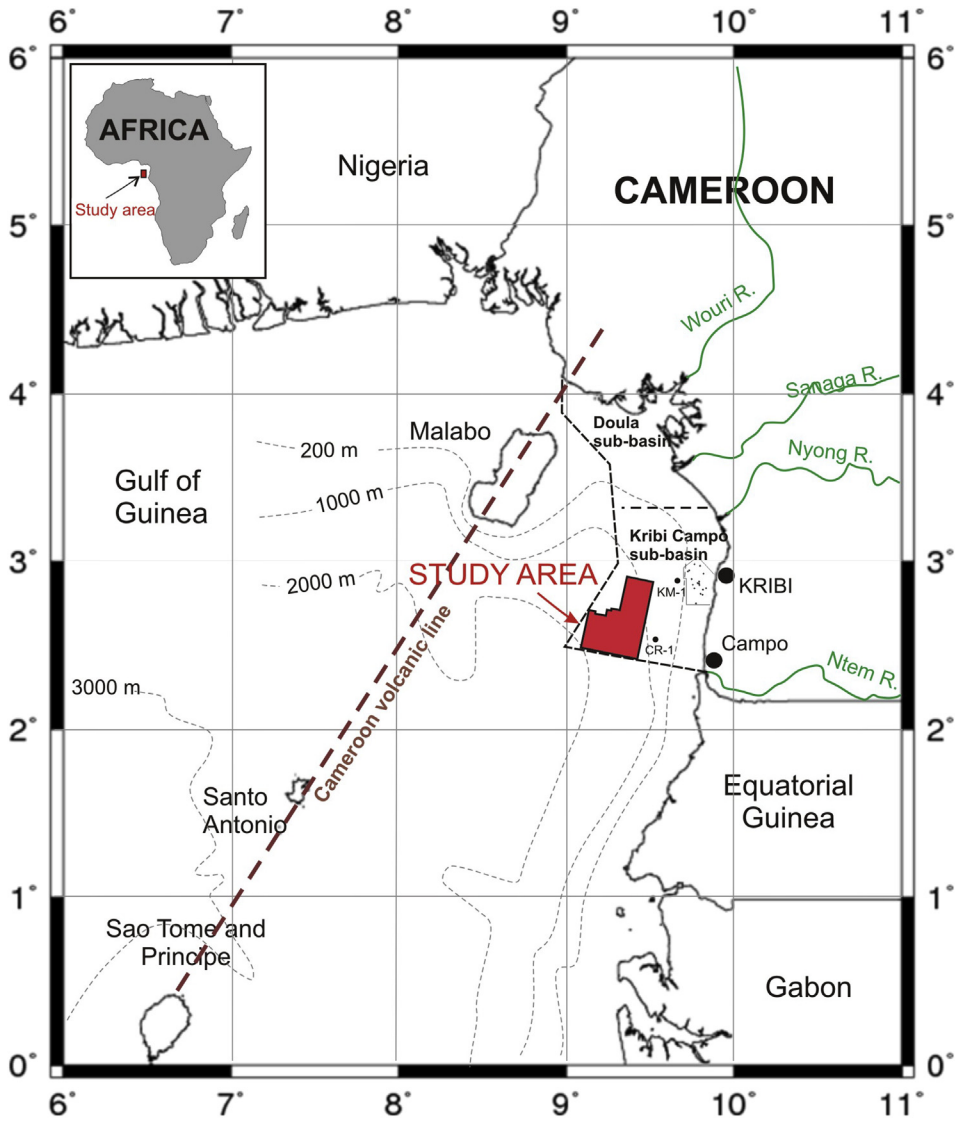

Figure 1. Location map of Cameroon margin (West Africa) shows the study area (in red). The area is located between 2°20′ N to 3°00′ N latitude and 9°00′ E to 9°50′ E longtitude. It lies about 40 km offshore Cameroon, in the Kribi-Campo sub-basin, at the water depth range from 900 to 2000 m. A number of wells have been drilled in the continental shelf. The map is complied from (Pauken, 1992; Meyers et al., 1996, Ntamak-Nida et al., 2008) and National Geophysical Data Centre (NGDC) for coast line. (For interpretation of the references to colour in this figure legend, the reader is referred to the web version of this article.)

is only about 45 km^2 and has a triangular shape (Ntamak-Nida et al., 2008).

The Kribi-Campo sub-basin is one of several divergent margin basins along the West African continental slope, formed as the result of the rifting that split Africa from South America during the breakup of Gondwana (Pauken, 1992; Binks and Fairhead, 1992). This continental rifting propagated from the South to the North, commencing in the Late Jurassic and lasting until the onset of seafloor spreading in Albian – Cenomanian time. Rifting started in the Kribi-Campo sub-basin from Barremian to Aptian time corresponding to deposition of the lower Mundeck formation (Ntamak-Nida et al., 2010). The Kribi-Campo sub-basin is thought to have been part of the Rio Muni, North Gabon and Sergipe-Alagoas (South America) rift branch of the proto-Atlantic (Davison, 1999; De Matos, 1992; Dailly, 2000) and they all have a broadly similar tectono-stratigraphic history (Dailly, 2000).

The important succession for the gas hydrate study is Pliocene to Pleistocene–Holocene strata, with a thickness of c. 600 m estimated from seismic data. No lithological data are available from the deep-water area studied. On the adjacent shelf, lithological description of borehole cores indicates that the Pliocene is made up of calcareous sandstone and occasional shelly limestones (Benkhelil et al., 2002). The Pleistocene sequence consists of alternating layers of silty sand and clayey sand (Benkhelil et al., 2002). Abundance of gas released by methanogenesis has been observed around the coast in the form of 'bubble muds' (Giresse et al., 1995). During the last eustatic low-stand (~19,000–20,000 years ago), radiocarbon datings suggest that sea level on the Cameroon continental shelf may have been lower than the present level by 135 m rather than the 120 m usually accepted on Gabon–Congo shelves to the south (Giresse et al., 1995).

The presence of a BSR related to gas hydrates has been widely reported offshore West Africa, at water depths greater than 1200 m, on the continental slope off the Niger and Congo River Delta, covering approximately 11,000 km^2 and 4000 km^2 respectively (Cunningham and Lindholm, 2000). Most gas hydrate provinces are associated with channels, pipes and pockmarks identified from seismic that are interpreted to form the migration network. They have been documented in many areas, such as the Niger delta front (Hovland et al., 1997; Brooks et al., 2000), Nigeria Continental Slope (Sultan et al., 2010), Equatorial Guinea (Pilcher and Argent, 2007), lower Congo basin (Gay et al., 2007; Andresen and Huuse, 2011), lower Kwanza Basin (Serié et al., 2012), Namibia (Swart, 2009; Moss and Cartwright, 2010b).

3. Methods and data

This study uses a high-quality 3D seismic reflection dataset from the offshore Cameroon margin. It covers an area of c. 1500 km^2, in water depths ranging between 600 m and 2000 m. The 3D seismic data include 1580 inlines and 2050 crosslines, with a bin spacing of 25 m. Standard seismic processing was applied to produce zero-phase seismic data. The positive and negative impedance contrast is displayed as red and blue colour on seismic displays, respectively.

The total thickness of stratigraphic succession overlying the basement is up to ~6.0 s TWT. We focus on c. 1 s TWT beneath the seabed. Time to depth conversion was not carried out for the entire dataset due to lack of accurate velocity information. Therefore, where depths are quoted, these have been calculated using the standard seawater velocity of 1.5 km/s, a shallow sediment velocity of 1.6 km/s and a typical velocity of 1.8 km/s for the hydrate bearing sediments in this shallow section. The dominant frequency of the near-surface seismic data ranges from 44 Hz to 48 Hz. It follows that the vertical seismic resolution is of the order of 8–10 m.

Measured geothermal gradients of shallow marine sediments in Congo, Gabon, Angola, Namibia margins are known between 45 °C/km to 57 °C/km (from ODP Leg 175 data) (Wefer, 1998). Deep water offshore Cameroon is a new exploration area where, due to a lack of well data, the geothermal regime is poorly constrained. Here we choose the geothermal gradient of 51 °C/km to estimate the conditions for gas hydate stability.

Interpretation has been carried out using Petrel software using a 125 m × 125 m interpretation grid; auto-tracking was then used on all the surfaces and resulted in good quality surfaces. Dip maps and attribute maps were generated of all surfaces to facilitate detailed geomorphological analysis.

4. Seismic stratigraphic analysis

4.1. Areal distribution

The study area is characterized by a gently sloping continental margin (seafloor gradient is less than 3.4°), located offshore approximately 40 km to the coast line. The slope can be sub-divided into a High Gradient Slope (HGS) dipping westward (1.6°–3.4°) and a Low Gradient Slope (LGS) dipping southwest (0.7°–2°), indicated by a line trending northeast–southwest along the centre of the study area (Figs. 2 and 3). This separation is based on the change of slope gradient, dip direction and differences in seismic facies and structures. The HGS covers an area of about 500 km^2 in the southeast of the study area, whilst the southwest dipping LGS covers an area of c. 1000 km^2 (Fig. 2).

4.2. Internal seismic stratigraphic sub-division

This study is focused on the shallow section, from Pliocene to seafloor. It is divided stratigraphically into two units, Unit 1 and Unit 2, based on a combination of seismic reflection character and terminations; and attributes of the bounding surfaces (Fig. 4).

Unit 1 is situated at the base of the shallow section and extends across the whole of the study area (Fig. 4). The sequence has a maximum thickness of c. 400 m in the LGS, thinning towards the HGS (Fig. 4). It is bounded by two unconformities, at its base by key surface KS_10 (a bi-directional downlap surface) and above by KS_20 (an onlap surface) (Fig. 4). The basal surface (KS_10) is characterized as a negative, high amplitude, continuous reflection. The top surface (KS_20) is a positive reflection with strength varying considerably across the two slopes; it is a high amplitude reflection in the LGS and a low amplitude reflection in the HGS. The unit is composed of low to high amplitude, continuous and discontinuous reflections. The most obvious difference in seismic facies within this unit is the reflection amplitudes. It is high in the LGS but low in the HGS. In more detail, the LGS is general characterized by sub-parallel, low continuity reflections that alternate between high amplitude and weak to seismically transparent; The HGS is characterized by parallel, low amplitude reflections with poor continuity. To identify and interpret the features associated with the high amplitude reflections of the LGS, this succession is further divided into 6 sub-units by 5 horizons (i.e., units A–F), based on changes in reflection strength and geometry (Fig. 5), and maximum amplitude maps of each unit have been generated (Fig. 6). The sequence is likely to be Pliocene in age based on the well correlation to the Sanaga Sub field (from Sterling Energy company internal report – 2002). As no direct calibration is available, the exact ages cited herein are subject to change.

Unit 2 is situated at the top of the shallow section, and bounded at the base by KS_20 and at the top by the seabed reflection, which displays an erosional truncation (Fig. 5). Unit thickness is relatively uniform, averaging c. 200 m (Vp = 1600 m/s). It is dominated by

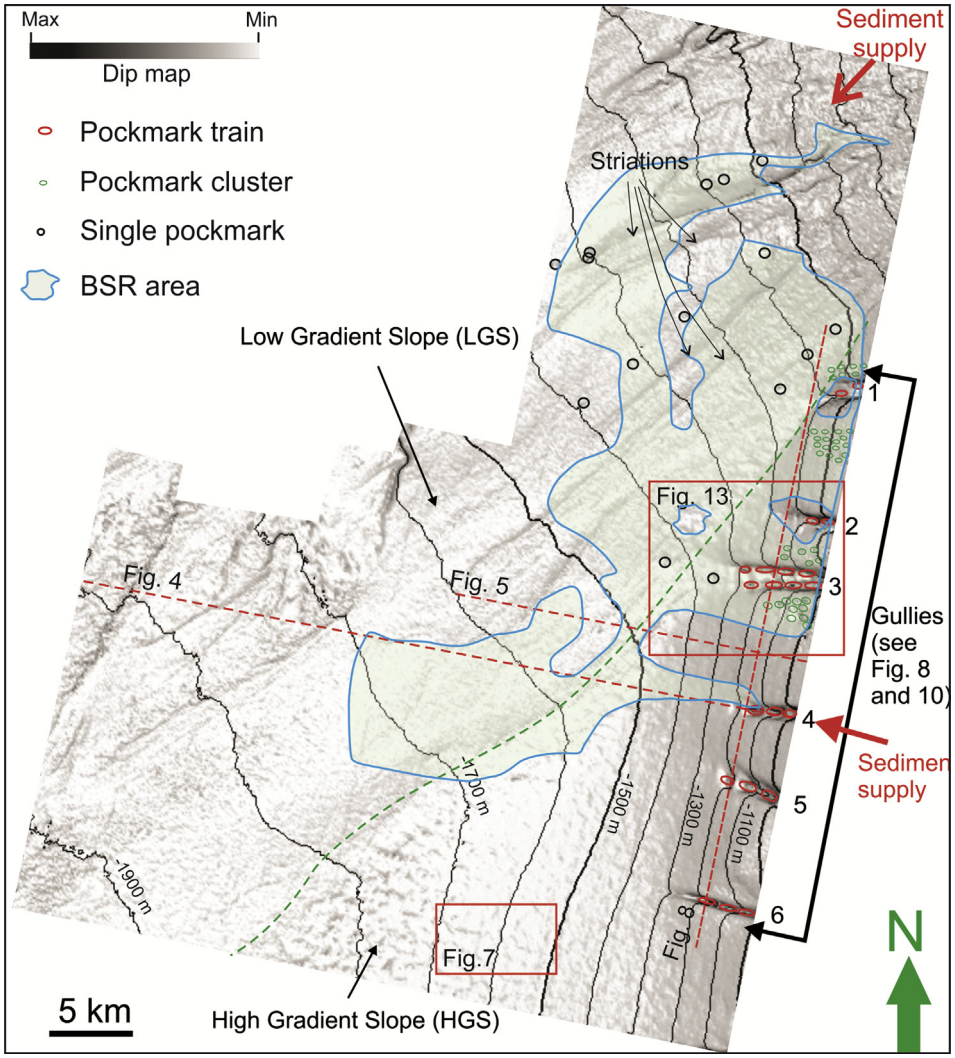

Figure 2. Sea bed dip map of the study area illustrating two defined sub-slopes: west dipping high gradient slope (HGS) and southwest dipping low gradient slope (LGS). Six parallel gullies located in the HGS cut down into the seafloor and terminate downslope. Detailed view of the location of pockmarks of the study area plotted on the seabed dip map. Single pockmarks are only developed in the LGS and located inside the BSR area or above the vertically stacked channels. All of the pockmark trains occur inside the gullies in the HGS. Pockmark clusters tend to be associated with pockmark trains and gullies. They appear as small scale pockmarks at the steepest dip of the HGS. See Fig. 13 for un-interpreted versions. Locations of subsequent figures are shown.

low amplitude, moderate to low continuity, sub-parallel reflections. High amplitude reflections are observed, but only locally developed. One internal horizon (KS_21) below the seafloor (c. 50 ms TWT) mapped within the unit characterized as a negative, high amplitude and continuous reflection. It mainly extends across the LGS (Fig. 4). This unit is interpreted to be Pleistocene – Holocene in age (from Sterling Energy company internal report – 2002).

4.3. Seismic facies analysis and interpretation

4.3.1. Pliocene – Unit 1

Two distinct facies are recorded in Unit 1: high amplitude reflections in the LGS correspond to a deep-water slope channel system and low amplitude reflections in the HGS are associated with polygonal fault systems. Aspects of these features are described in more detail below.

a. Polygonal faults in the HGS. The time structure map of an internal horizon in Unit 1 of the HGS reveals the presence of numerous steeply dipping discontinuities (Fig. 7). They are all closely spaced normal faults with a throw of 10–20 ms TWT, 100 m–1000 m spacing, with a polygonal plan view expression (Fig. 7) and mainly dip counter to the regional slope at a dip of around 60° (Figs. 4 and 5). These faults are interpreted as layer-bound polygonal faults (Cartwright and Dewhurst, 1998; Cartwright, 2011). The polygonal fault tiers are delimited by regionally correlatable stratigraphic surfaces (KS_10 and KS_20). This form of compaction-related faulting is considered to be the result of lateral sediment contraction and pore fluid expulsion. They are mainly developed in passive margin basins and typically occur in fine-grained sedimentary sequences (<2 μm) (Cartwright and Lonergan, 1996).

b. Pliocene fan–channel complex system in the LGS. Maximum amplitude maps generated from units A to E consistently reveal northeast–southwest trending high amplitude features within the LGS (Figs. 5 and 6). The high amplitudes display channel-like morphologies, c. 1–5 km wide, 20–40 km long, which at the large scale starts rather straight and then becomes smaller and more sinuous in the younger units gradually migrating eastwards.

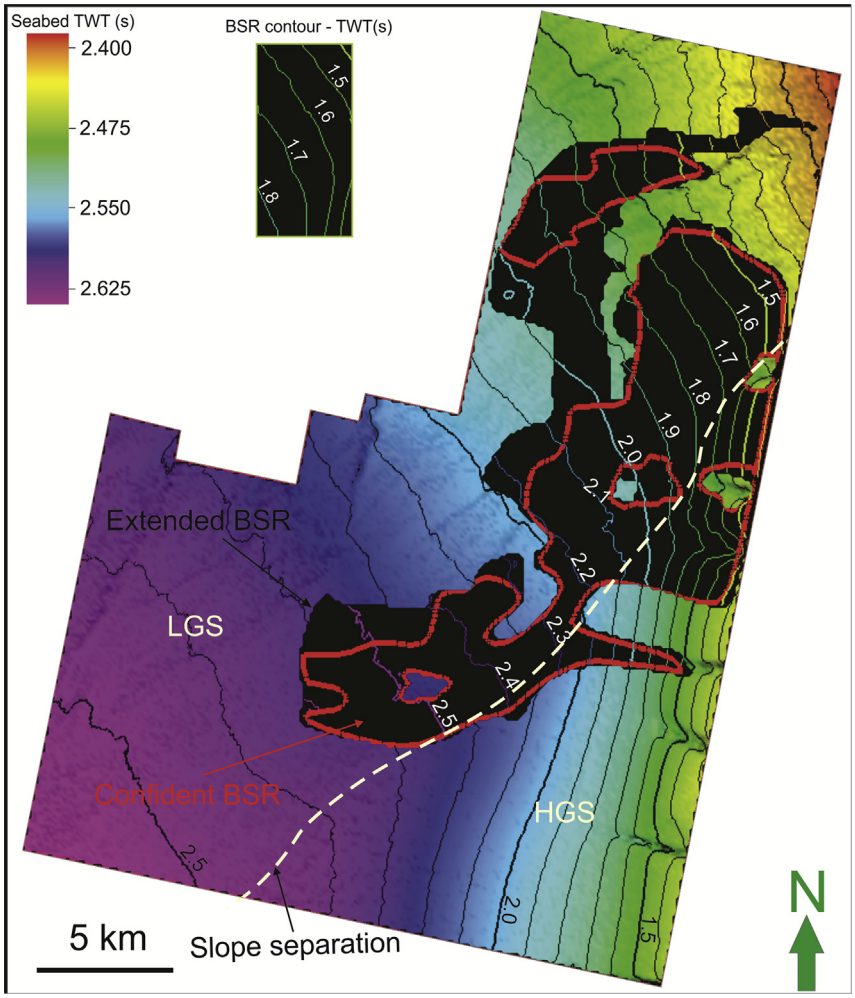

Figure 3. Distribution of the BSR is placed on the seabed TWT map. The unfilled contours in the centre of the study area showing the area of BSR (TWT) mapped; high confident mapped BSR is bounded by red polygon. The BSR increases in depth with increasing water depth. (For interpretation of the references to colour in this figure legend, the reader is referred to the web version of this article.)

In the lowest Unit (unit A), the channel-like morphology is relatively straight, increasing in amplitude and width down-slope (Fig. 6a). Channel width increases from 3 to 5 km and it extends for c. 55 km crossing LGS, from northeast to southwest. Internally it is composed of low to high amplitude, continuous upward-convex reflections with bi-directional downlap onto the key surface KS_10 (Fig. 4). In cross-section, the feature is dome shaped, and combined with its planform geometry. It is interpreted as a low-sinuosity channel. The domal cross section is most likely due to differential compaction between the coarser (sandy) channel fill and muddy substrate and levees. A wider high amplitude pattern downslope and bi-directional downlap suggests a downslope transition from channel to fan lobe deposits commonly found in deep-marine clastic systems (Stow et al., 1996).

In the younger Units (B–E), northeast–southwest trending high amplitude features are observed, which are smaller and have a higher sinuosity compared with the straight channel in Unit A. They are c. 1–3 km wide, vary from 20 to 40 km in length and widen downslope. The sinuosity is observed to increase upwards in the younger channels (Fig. 6b–e). In cross-section, the features show a 'U' shaped profile and up to 250 ms TWT relief (Fig. 5). These high amplitude features extend from the northeast or east and continue downslope. They are developed in a zone flanked on one side by the oldest channel (in Unit A – Fig. 6a) and on the other side by the HGS. They are interpreted as a series of sinuous channels which are constrained within a northeast–southwest high amplitude zone interpreted to be a channel complex system. Channels are not observed in the youngest level (Unit F – Fig. 6f).

The channel complex shows horizontal and vertical amalgamation. It was fed by two sediment sources, one to the northeast and the other to the east (Fig. 6). The boundary of the channels are observed to evolve by eastward migration, shifting laterally, and running parallel to and being limited by the boundary of the HGS.

In the central basin, the Pliocene channel complex contains three channels stacked sub-vertically to vertically. They extend from the upper HGS, associated with gully 3, then re-direct, following the LGS gradient. In cross-section, they clearly show 'U' shaped, erosional bases with very bright amplitude onlap fills (Fig. 5). In map view, they are about 4 km in width, c. 30 km long and c. 120 m deep. These stacked channels extend from the HGS to the east. Once reaching the LGS, they flow down the LGS and follow the transition of the two slope domains.

In summary, abrupt changes in the seismic character of the HGS and the LGS are likely caused by differences in lithology and lithofacies successions. Low amplitude reflections and the presence of polygonal fault systems in the HGS are indicative of uniform, fine-grained deposits such as hemipelagic or pelagic sediments. High amplitude reflections dominant in the LGS, interpreted to be a

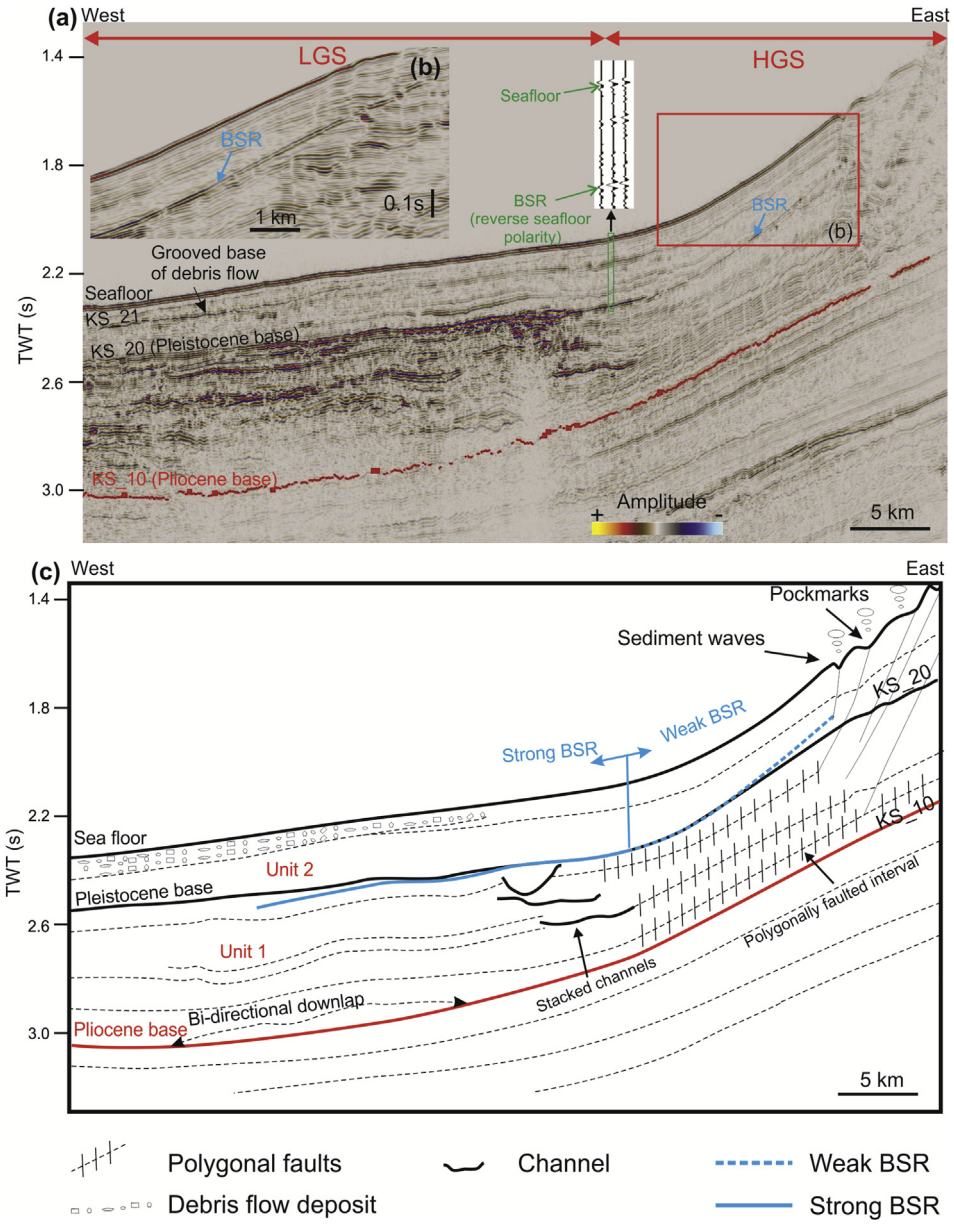

Figure 4. Seismic profile downslope along gully 4 and interpreted line drawing illustrating overview of the stratigraphy and main structural elements of the study area, defined by two slopes, High Gradient Slope (HGS) and Low Gradient Slope (LGS) (see Fig. 2 for the location map). In unit 1 (from KS_10 to KS_20), the LGS is characterized by the alternation of low to high amplitude reflections associated with the vertical stacked channels; the HGS shows low amplitude reflections associated with the polygonal faults and E-flowing gullies which associated with sediment waves. The upper unit (from KS_20 to the seafloor) is dominated by low amplitude reflections in both slopes. While the LGS is highly modified by the debris flows and sliding, the HGS experienced less deformation but does contain a gully system.

fan–channel complex system, with higher amplitudes suggesting abundant coarser grained sediments compared with the HGS.

4.3.2. Pleistocene – Holocene – Unit 2

Unit 2 is top of the shallow section and probably of Pleistocene–Holocene age (Fig. 4). Seismic facies analysis reveals slope failure is intensive, occurring on both slopes, forming abundant gullies in the HGS and slump deposits in the LGS. Details of them are described below.

a. Gully system in the HGS. The seabed dip map reveals 6 parallel, linear, 'U' shaped incision features in water depths of 1100 m–1300 m, trending east–west across the HGS. They extend from the upper slope for c. 3–6 km, and are about 1.5 km wide and c. 100 m deep with steep flanks (50°–60°) (Figs. 2 and 8). The base of the gullies is characterized by series of pockmarks extensively developed with close spacing (Fig. 8) (described in detail in 5.2).

In cross section, buried gullies can be seen underneath the seabed gullies (Fig. 8a). They appear to be long-lived features, developed from the Pliocene or Pleistocene up to the present day, increasing in width upwards (Fig. 8a). Gullies and inter-gullies are characterized as aggradational reflections dominated by low amplitudes. Core calibration available in inter-gully areas in Gabon and Equatorial by Jobe et al. (2011) show that these consist of fine-grained deposits, while these authors interpret uncalibrated gully areas from their seismic character to consist of coarse-grained deposits. Jobe et al. (2011) also classified the gullies as 'Type II' canyons, characterized as mud-rich with occasional sand where the

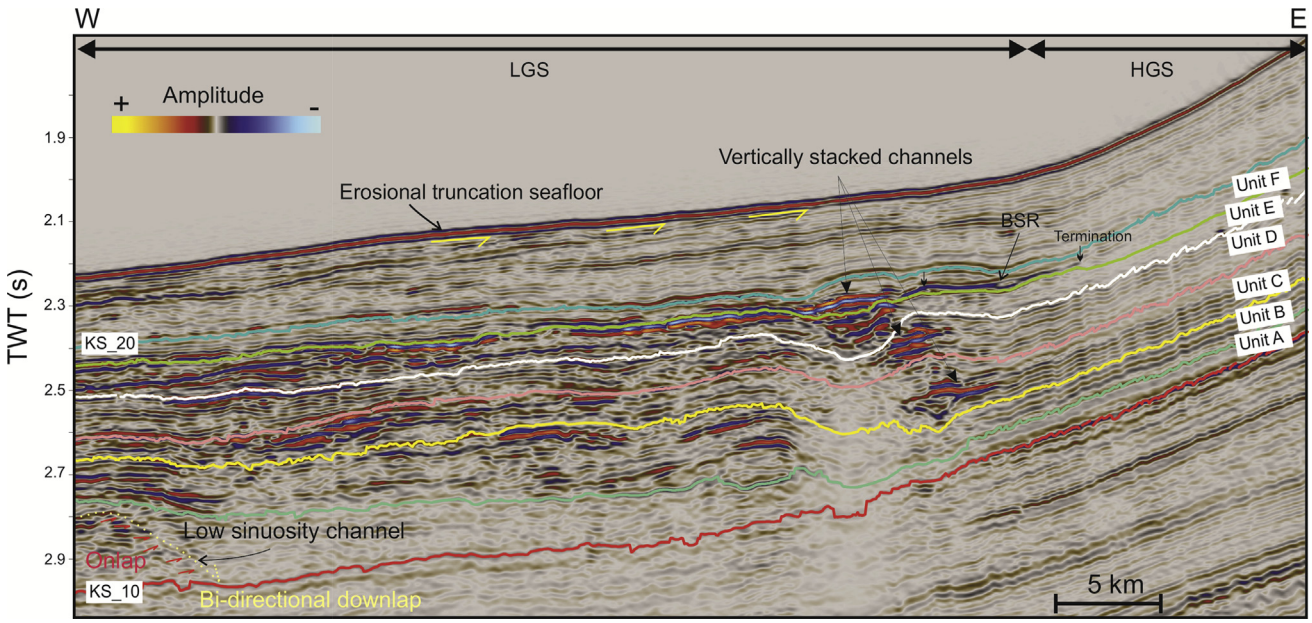

Figure 5. Seismic cross-section showing 5 sub-horizons of the Unit 1 (between KS_10 and KS_20) which subdivides the unit into 6 intervals marked from A to F. See Fig. 2 for line location and Fig. 6 for internal attribute maps of each sub-unit.

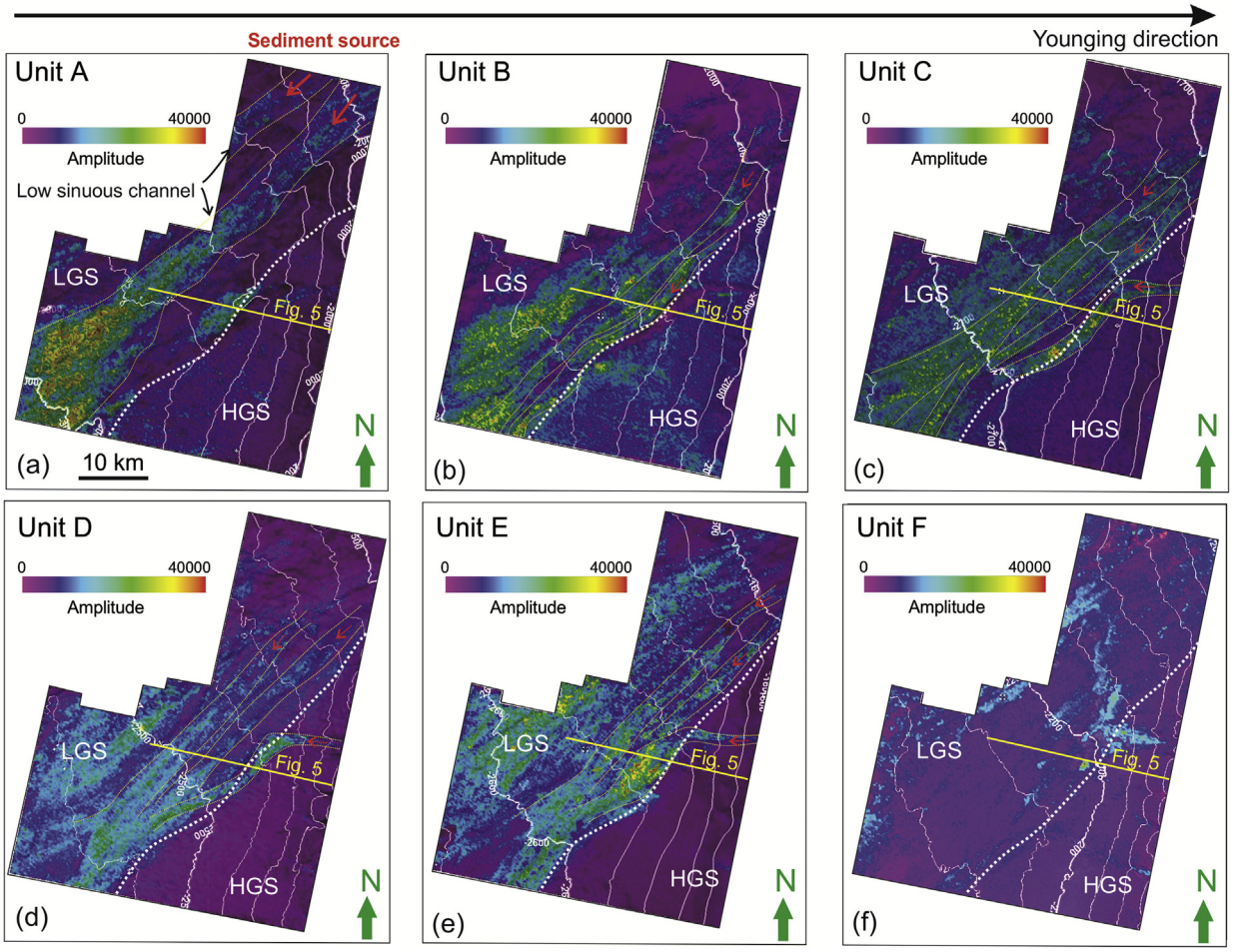

Figure 6. Maximum Amplitude map of each sub-unit A to F display in the map from 6a to 6f, respectively, reveals a fan–channel complex system developed in the LGS. Starting with large scale and rather straight channel in Unit A and increasing sinuosity and decreasing scale. It almost disappears in Unit F.

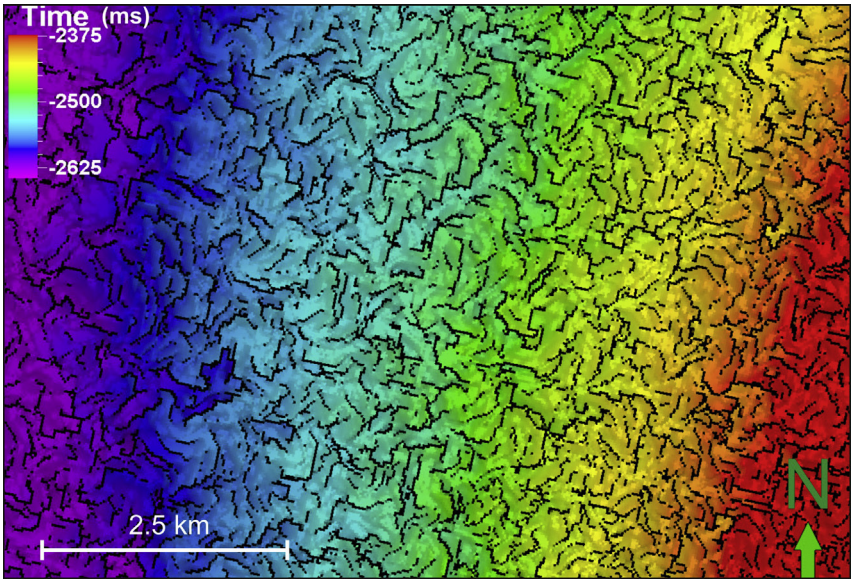

Figure 7. TWT time map of one internal horizon within unit 1 showing the polygonal fault system in the HGS. They are closely spaced, normal faults with a throw of 10–20 ms TWT, spacing <700 m, mainly dip upslope. See Fig. 2 for the location.

high amplitude reflections present and mainly developed in areas of low sediment supply which are aggradational rather than erosional.

Overall, in the HGS, the modern seafloor is intensively modified by a number of gullies, which have developed since the Pleistocene. Decreasing gully scale with greater depth may be due to compaction which will reduce sediment volume by water loss and will cause decrease in height of the paleo-gully margins. In addition, compaction will also result in increase seismic velocity, thus resulting in smaller scale of gullies. In marine sediments, clay-rich sediment will decrease initial porosity from 75 to 90% to nearly 40% at about 500 m depth (Velde, 1996). It almost reduces porosity by a half, thus resulting in thinner sediment layers.

b. Sediment waves associated with the gullies. Dip seismic sections of individual gullies reveal distinctive seafloor and subsurface undulations (Fig. 9). The undulations are confined to within the gullies and display a staircase-like morphology (Fig. 9). The wavelengths

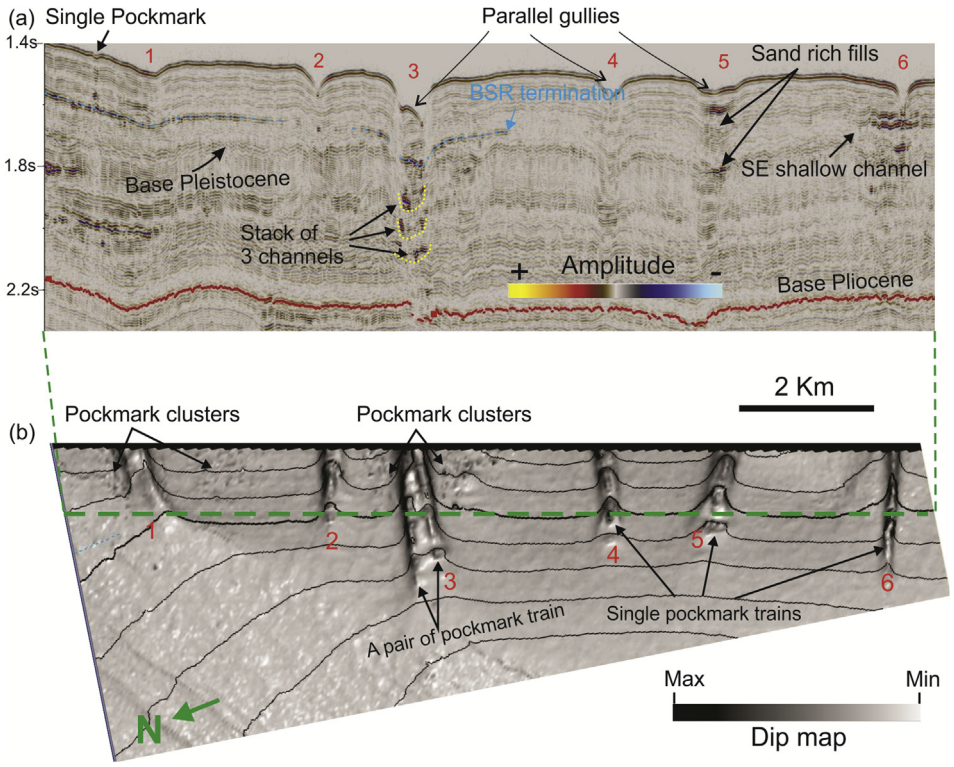

Figure 8. (a): Seismic section showing all of the gullies in the HGS and their image on a seabed dip map (b): Gullies are marked from 1 to 6; individual gullies are associated with either a single pockmark train or a pair of pockmark train. A pair of pockmark trains is only observed in the gully 3. See Fig. 2 for the location and Fig. 4 for the dip sections of the gullies.

from the seafloor to sub-surface are almost the same scale (0.5 km–1 km) but amplitude varies significantly from ~30 to 40 m on the seafloor to ~10–20 m in the subsurface. The undulations tend to decrease in amplitude and wavelength downslope. Consecutive reflections show an aggradational to landward migrating crest of the undulations. Truncations are locally observed underneath the undulating reflections (Fig. 9). The boundaries between the undulations are dipping downslope at angles of 6°–25° (seafloor surface dips gently at ~3°). These undulating reflections are mainly developed in the Pleistocene unit but is also detected at deeper levels of likely Pliocene age.

The geometry of the apparent discontinuities between the undulations could be interpreted as deformation (faulting) due to gravitational slope movement. However, there is no clear evidence for the reflections being offset through the boundaries (Fig. 9). In addition, the boundaries between the undulations are dipping at much lower angles (average 10°) than the friction angle (~60°) to initiate the slope failure or sediment deformation. This issue has been robustly discussed by Berndt et al. (2006) to point out the necessary angle of fault if it is to be interpreted as a result of deformation. Moreover, if the extension occurred to generate normal faults, there would be expectation of the compression downslope, at the termination of the faults. But there is no evidence for that. More importantly, several truncated undulation surfaces are locally observed, which supports the sediment wave interpretation.

Decreasing wavelengths and amplitudes seaward combined with its restriction within the gullies and also truncated undulation surfaces suggest for fan origin as turbidity current sediment waves, similar to those described and classified by Wynn and Stow (2002). The trigger for the development of sediment waves could be pre-existing roughness of the seabed topography, that could mark the

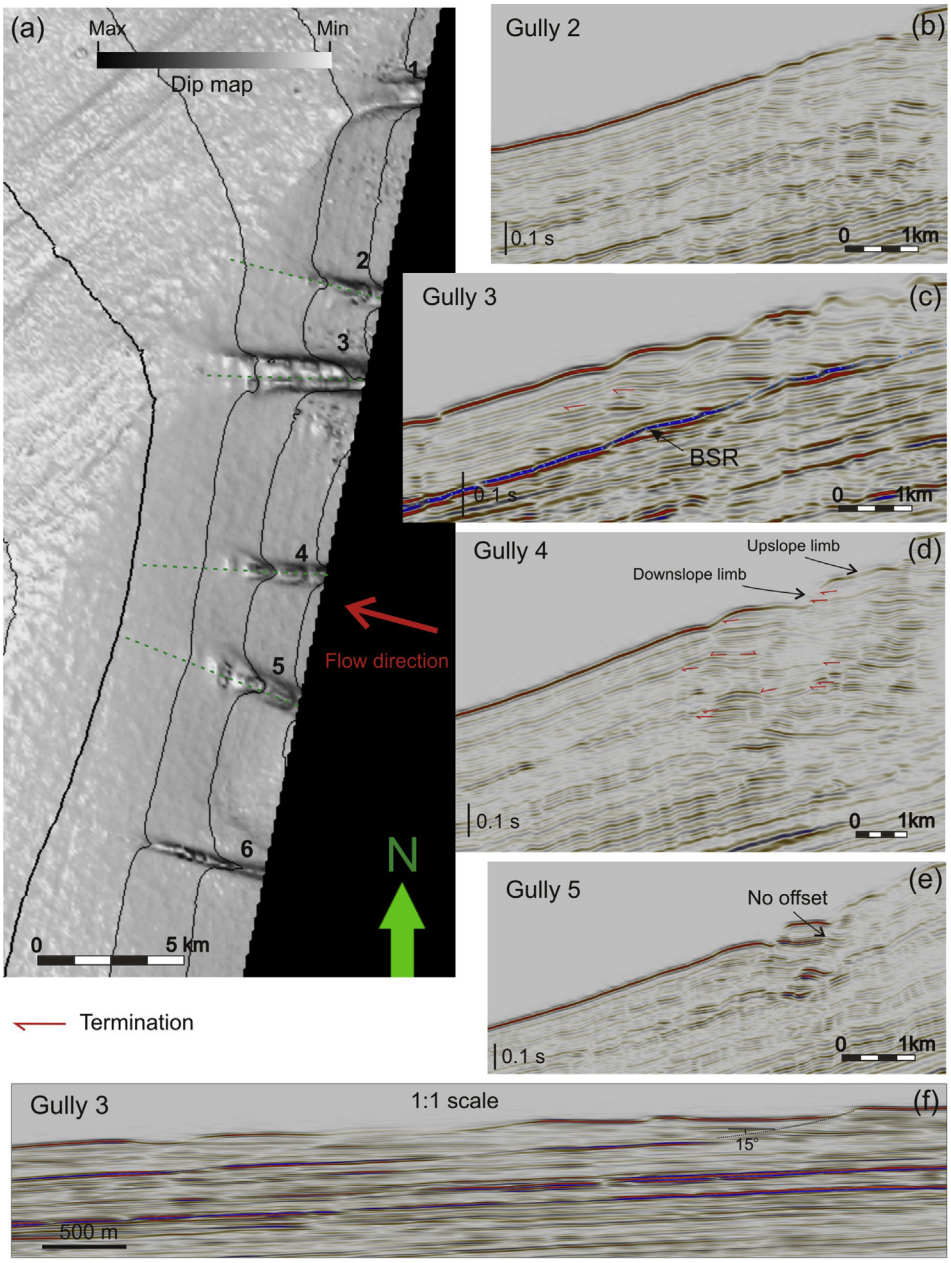

Figure 9. Seafloor dip map showing HGS gullies and seismic line locations (b–f). Seismic lines illustrating length profiles of each seafloor gully. Gullies are associated with the sediment wave deposits.

lateral change in sediment accumulation rates, or the roughness of the seafloor topography could be created by the instability of the flow itself (Kubo and Nakajima, 2002). The difference between present day and paleo-sediment wave heights is interpreted to be due to the compaction at depth and increasing in seismic velocity, and also recent strong erosional processes active on the seafloor (sliding and gullying).

c. Striation surface in the LGS. Within the Pleistocene unit, reflection KS_21 (at about 50 ms below the seafloor) is notable in that it displays large scale, well preserved, parallel striations (Fig. 10), extending across an area of c. 150 km^2 from the upper LGS to the deep basin area. Individual striations are 20–50 m wide, c. 10 km long and 4–8 m deep, slightly curving from the north-east toward the south-west. There is no obvious divergence in the striation patterns. In cross-section this reflection marks the base of a mixed low to high amplitude, chaotic, discontinuous reflection package (Fig. 10b). Similar striations are also observed on the seafloor, at a larger scale but exhibiting the same trend (c. 2 km wide and c. 15–20 km long with a relief of 12 m) (Fig. 2). The origin of the striations is interpreted to be scour beneath a submarine landslide (Piper et al., 1988; Gee et al., 2005), highlighting the importance of landsliding for re-sedimentation processes in the LGS.

In summary, The Pliocene–Pleistocene units represent the youngest deposits on the slope of the Kribi-Campo sub-basin. The active depositional system is interpreted to be largely influenced by slope processes, with the recognition of channels, sediment waves, gullies and slide surfaces. The recognition of striations on the seafloor and a shallow buried striation surface on the KS_21 in the LGS reveal significant recent slope instability.

5. Fluid-related features

5.1. Bottom-Simulating Reflection (BSR)

5.1.1. Seismic expression

An anomalous seismic reflection is observed in the Cameroon continental slope at about 200 ms TWT below the seafloor. The reflection is characterized by the following observations:

1. The reflection cross-cuts the primary stratal reflections and is sub-parallel to the seabed on a regional scale (Fig. 11).
2. The reflection has reversed polarity to the seafloor (Fig. 4) and variable amplitude (Fig. 12b).
3. The reflection is characterized by an increase in depth below the seafloor with the increasing water depth (Fig. 11), except in the gully area, which does not follow the main trend and will be

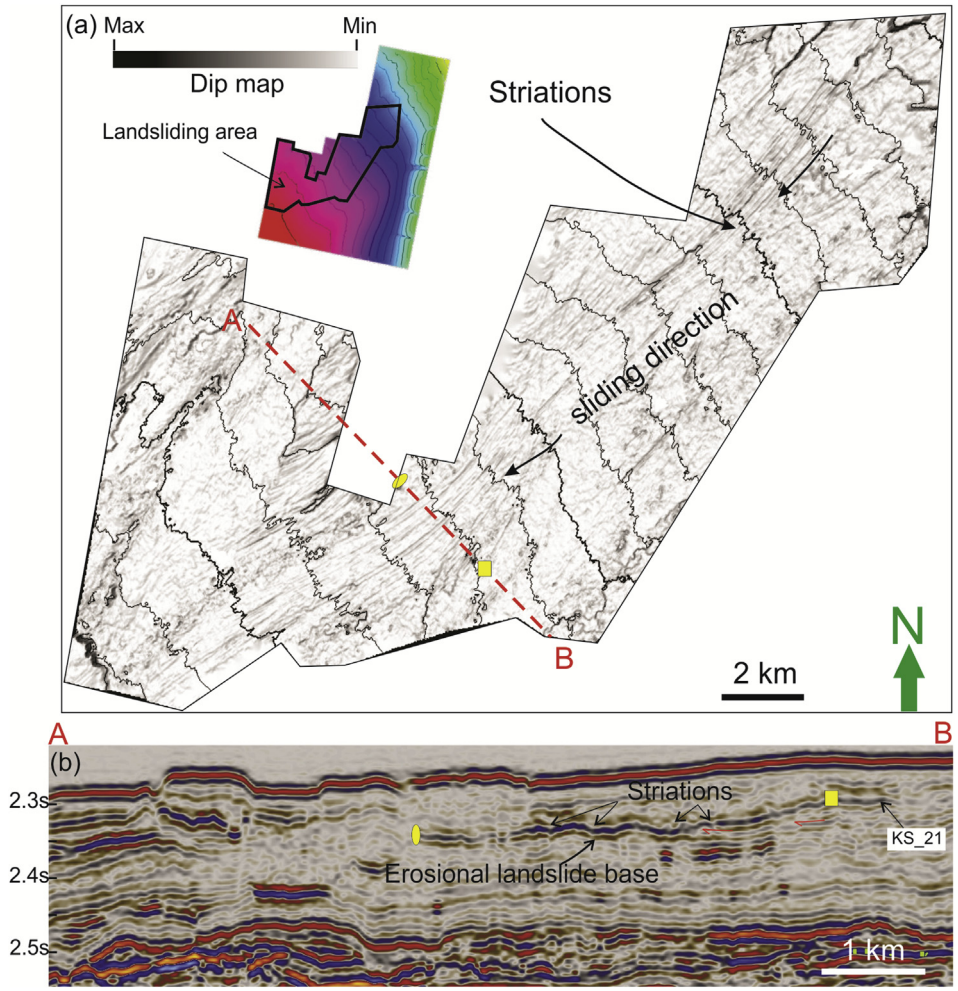

Figure 10. (a) A dip map along horizon KS_21 showing striations extending c. 150 km^2 in the LGS, slightly curving from the north-east toward south-west. (b) A seismic section across the LGS illustrating the KS_21. The horizon is characterized as a strong reflection, marked the base of mixture high and low amplitude, chaotic, discontinuous reflection package. KS_21 is interpreted the base of a sub-marine landslide.

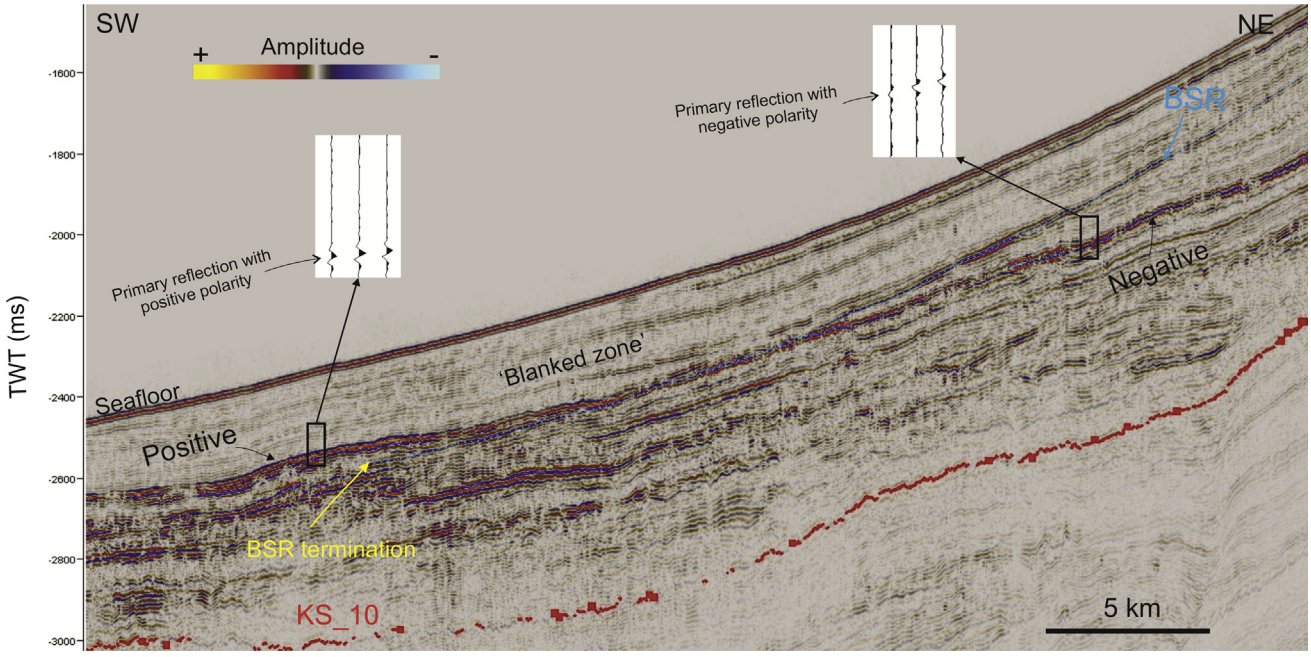

Figure 11. A seismic cross-section along the LGS showing the BSR cross-cuting primary reflections, and the change of acoustic impedance contrast of the primary reflection from negative polarity to positive polarity when it crosscuts the BSR. See Fig. 12 for the location.

discussed later. Depth of the reflection below the modern seafloor varies between 126 m and 235 m.

4. 'Blanking' or reduction of seismic amplitudes above the reflection compared with the reflection amplitudes below is observed in both slopes (Fig. 11).
5. Locally, the polarity of stratal reflection change when crosscut by the reflection (Fig. 11).
6. The area of the anomalous reflection broadly coincides with the area of abundant seabed pockmarks (Fig. 2)
7. The reflection is pulled-up where fluid pipes go through it and pushed-down below the sea floor gullies (Fig. 13)

5.1.1.1. Interpretation. Anomalous seismic reflections that cross-cut sedimentary strata are generally related to post-depositional geological processes or fluid migration (Berndt et al., 2004). Based on the criteria defined by Berndt et al. (2004), the above characteristics are interpreted to indicate the presence of a Bottom

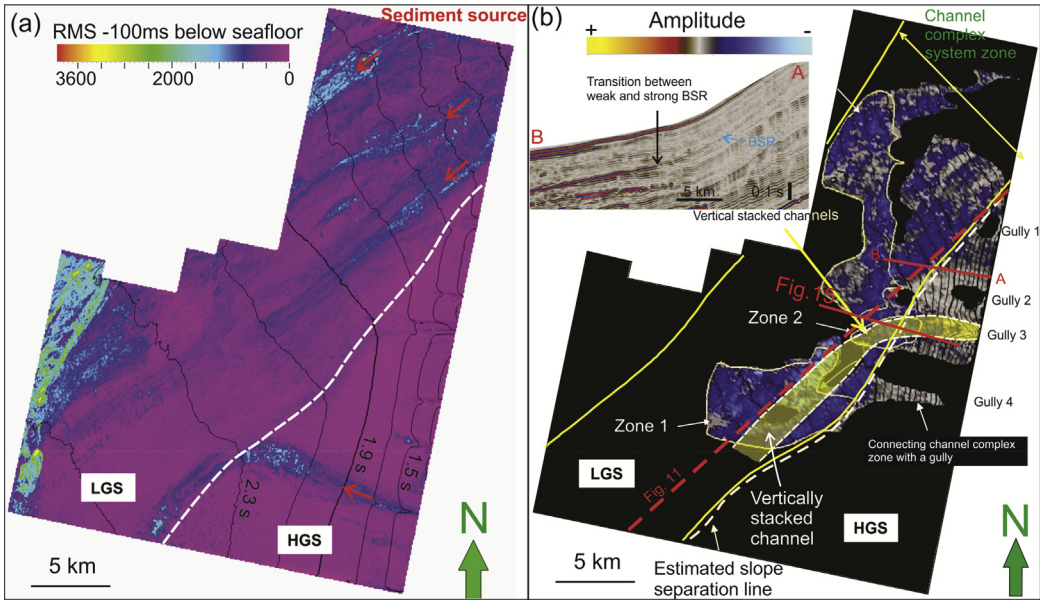

Figure 12. (a) RMS of 100 ms below the seafloor showing the recent sediment source is still from Northeast and east which is consistance since Pliocene; (b) Amplitude extraction of the BSR showing the extent and amplitude variation of the BSR (blue colour: strong BSR; grey colour: weak BSR). The BSR shows a very sharp change from a weak to strong reflection, going from HGS to LGS which is illustrated in cross-section AB. The strong BSR is associated with the fan–channel complex zone beneath the BSR trending northeast – southwest. Vertically stacked channels (highlighted in yellow) are part of this fan–channel complex system but it extends from east and is associated with the gully 3. Three zones are marked from 1 to 3 that illustrate the areas with high to bright amplitude reflections observed just above the BSR, detail shown in Fig. 15. (For interpretation of the references to colour in this figure legend, the reader is referred to the web version of this article.)

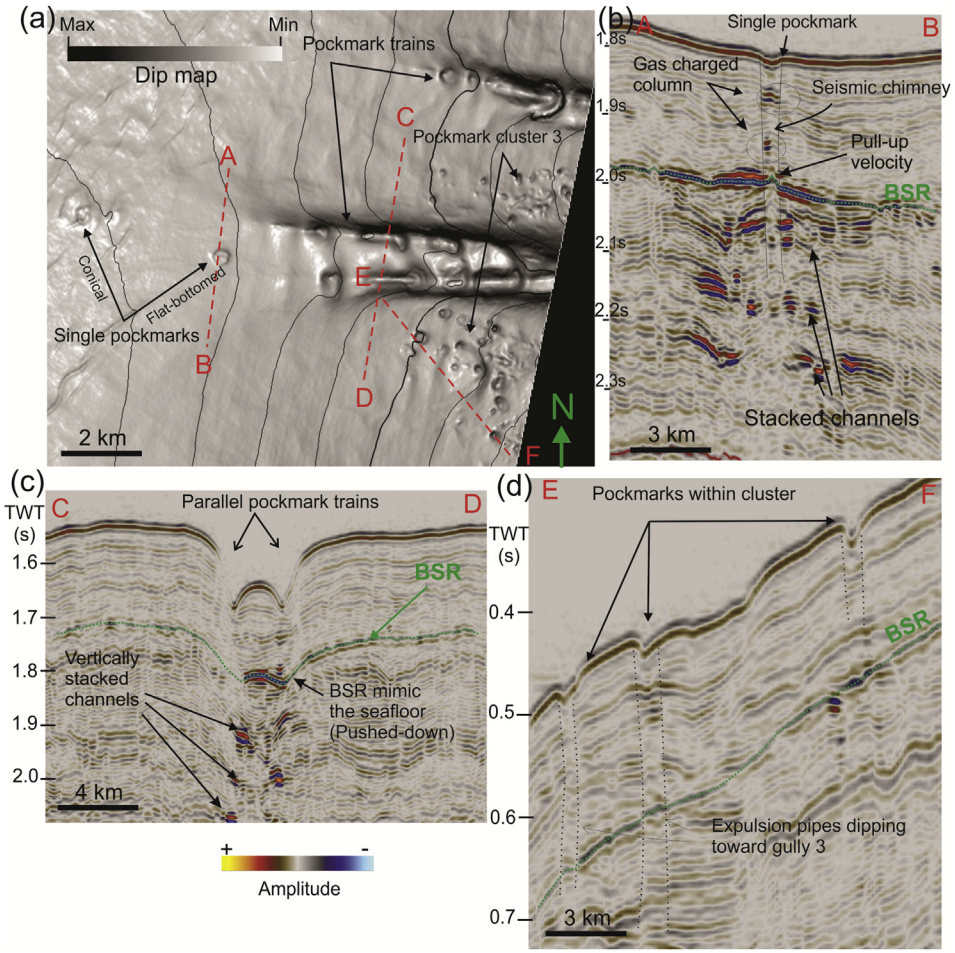

Figure 13. Seafloor dip map around gully 2 and 3 showing three types of pockmarks (a) and seismic cross-sections (b–d). (b) seismic cross-section illustrating single pockmark which is associated with a seismic chimney and vertical stacked channels. (c): seismic cross-section showing a pair of pockmark trains with sub-vertical fluid expulsion pipes. (d): seismic cross-section illustrates for the pockmark clusters (See Fig. 2 for the location of the dip map). (For interpretation of the references to colour in this figure legend, the reader is referred to the web version of this article.)

Simulating Reflection (BSR). The polarity of the reflection is key with regards to the specific origin of shallow subsurface BSRs. A deepwater BSR that crosscuts stratigraphy and mimics a dipping seafloor with opposite polarity to the seafloor is indicative of the gas-hydrate to free gas interface (Berndt et al., 2004). A methane hydrate-free methane phase diagram for the study area with the water depth range from 950 m to 1750 m is shown in Figure 14, with the chosen geothermal gradient of 5.1 °C/100 m.

5.1.2. Distribution and variation

The BSR covers an area of c. 350 km^2 within a water depth range from 940 m to 1750 m. The BSR occurs at a depth below the seafloor that ranges from 100 m–250 m, crossing the two slopes (Fig. 3). The BSR can be mapped beneath some gullies (especially gully 3) and is absent beneath others. The mapped BSR extent has been divided into two areas, one mapped with high confidence and one of low confidence. The high confidence BSR is defined by continuous reflections which show clear cross-cutting of primary reflections, sub-parallel and reversed polarity with relation to the seafloor. The low confidence BSR extends from the high confidence BSR further downslope to the LGS. In this area the BSR reflection is disrupted and no clear cross-cutting relationship can be observed in part because of the gentle dip of the sub-seafloor stratigraphy.

The strength of the BSR is not only controlled by presence of gas hydrate, but also depends on the presence of the free gas underneath it which is considered for the primary cause of BSR (e.g. Bünz and Mienert, 2004). BSR amplitude variations are clearly illustrated in our data (Fig. 12b). The observation of an increase in amplitudes associated with the Pliocene fan–channel complex system is located immediately underneath the BSR, is interpreted to be related to the presence of coarse grained sediment in the channels, which have higher porosity and thus store free gas below and higher concentrations of hydrate above, creating a high velocity across the BSR. This results in a strong BSR. In contrast, the weak BSR observed in the HGS is interpreted to be caused by limited free gas in the dominantly muddy HGS sediment thus reducing the velocity contrast.

In summary, the BSR is distributed in both HGS and LGS, covering almost of the study area. Its strength varies significantly from generally weak in the HGS to strong in the LGS.

5.1.3. Associated amplitude anomalies

Amplitude anomalies are observed as bright spots within the gas hydrate stability zone and manifest as velocity pull-ups on the BSR. They are only observed in the LGS (Figs. 13 and 15).

5.1.3.1. Bright spots within the GHSZ. The bright spots within the GHSZ are interpreted to be discrete layers of highly concentrated hydrate formed by upward migration of gas (Hornbach et al., 2003). The bright spots are found near the top of the Pliocene fan–channel

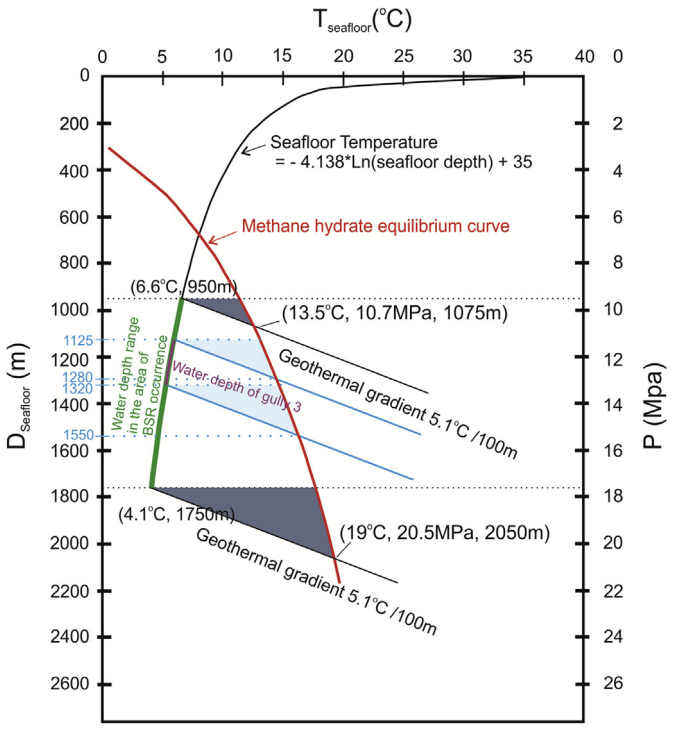

Figure 14. Seafloor temperature is shown as a function of depth in the study area. Seafloor temperature of this study is from 4.1 °C to 6.6 °C in the water depth range between 940 and 1750 m corresponded to the BSR area. The methane hydrate equilibrium curve (red) is a function of depth and temperature after Dickens and Quinby-Hunt (1997). Hydrates are only stable between the equilibrium line and the geothermal gradient to the left of the curved line (filled in blue). Two geothermal gradient lines correspond to the two end of the water depth range indicate the hydrate stability condition in the study area: T < 19 °C and P > 10.7 MPa. The average geothermal gradient of 5.1 ℃/100 m is taken from Ocean Drilling Program (ODP Leg 175) data which have most penetration depths less than 200 mbsf (Wefer, 1998). According to the phase diagram, within the gully 3, with the water depth range from 1125 m to 1320 m, the BSR will be expected at the depth of 1280 m–1550 m, respectively. (For interpretation of the references to colour in this figure legend, the reader is referred to the web version of this article.)

complex system and limited to the LGS. This indicates the presence of porous sandstones. The sands are interpreted to pinch out toward the HGS, resulting in loss of bright spots.

5.1.3.2. BSR pull-up. Pull up of the BSR is mostly observed in the LGS and is associated with single pockmarks (see 5.2) (Fig. 13b). BSR pull-up phenomenon can be produced by a number of causes such as fluid movement or velocity affects. The local high velocity anomalies directly above the reflection affected, producing apparent highs. This would be produced by a reduction in porosity, such as by carbonate cemented sandstones or a high concentration of gas hydrate above the BSR, both of which would result in high velocities (Gay et al., 2007; Hornbach et al., 2003). In addition, BSR elevation could be related to local variations of the thermal condition due to the fluid movement (focused fluids) upwards (De Batist et al., 2002; Gay et al., 2007; Pecher et al., 2010). Advection of heat through focused fluid flow causes locally higher temperatures (Ganguly et al., 2000; Shankar and Riedel, 2010; Le, 2012).

5.2. Seismic expression of pockmarks

Some of the most distinctive and interesting features observed on the seafloor are circular to oval seabed depressions which are interpreted as pockmarks caused by the deformation and blow out of seabed sediment by escaping fluids (Judd and Hovland, 2007). Three distinct styles of pockmarks can be recognised on the modern seafloor based on their distribution, size, shape and density. They are (1) single pockmarks, (2) pockmark trains and (3) pockmark clusters (Figs. 2 and 13).

Single pockmarks are only located on the LGS and appear as small depressions, some 300–400 m across (Fig. 13a,b). The internal shape of the pockmarks ranges from conical to flat-bottomed (Fig. 13a). They are observed within the BSR area, tend to be distributed either beside the slides, parallel with the sliding trend (black circles on Fig. 2) or overlying vertically stacked channels. Pilcher and Argent (2007) suggested that fresh pockmarks are conical depressions which become rounded or flat-bottomed through time due to slumping and or infill by hemipelagic sedimentation. In addition, Sultan et al. (2010) considered the flat-bottomed pockmarks as hydrate-related features which is a direct consequence of hydrate dissociation and excess pore pressure.

Pockmark trains are made up of linear strings of almost circular to elongate pockmarks (Fig. 13a), which are quite uniform in size and space, approximately 300–400 m in width, 1–1.5 km in length and with depths ranging from 10 to 35 m (Fig. 13c). Compared to the seismic resolution (horizontal: 25 m and vertical: 10 m), those features are not likely related to seismic processing/imaging. Pockmark trains may occur as single or paired downslope trending arrays. They are all located inside the gullies in the upper part of HGS at the location of steepest dips. Similar styles of pockmark trains have been reported offshore Gabon, Congo, West Africa by Pilcher and Argent (2007) and Gay et al. (2003).

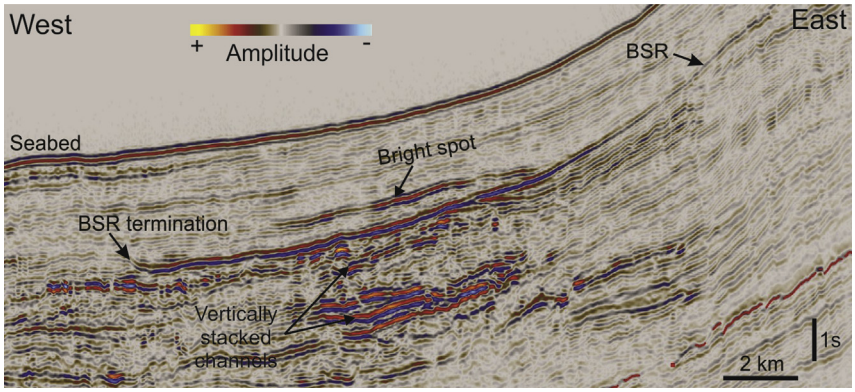

Figure 15. Seismic cross sections showing the relationship between the high to bright amplitude reflections and the BSR in the zones 2. They are all related with the fan–channel complex system in LGS. The high/bright amplitude reflections are c. 0–80 ms TWT above the BSR. See Fig. 12 for the location.

Pockmark clusters are made up of groups of pockmarks, which are closely spaced and relatively uniform in size and shape (Fig. 13a). Pockmark clusters are observed only beside the margins of some gullies and they are characterized by having almost circular to elliptical shapes ranging in diameter from approximately 50 m–250 m. The pockmark clusters closest to gully 3 have major axis directions which are mostly oblique to the trend of the gully (Fig. 13a and d). The expulsion pipes of other pockmark clusters show a generally downslope dip direction. The depths of the pockmarks range from about 7 m to 15 m. The pockmark density within the clusters is approximately 2 per km^2. The location and the expulsion direction of pockmark clusters suggest a relationship with the pockmark trains; possibly produced by the same migrating fluids.

Cathles et al. (2010) suggested that due to the density of methane under shallow sediment is c. 6 times less than water (200 kg/m^3 and 1025 kg/m^3), the main resistance to the upward migration of the gas chimney will be pushing water aside so gas can move upward. Therefore, gas pipe behave like fluid pistons moving vertically as a unit which is resisted by water being displaced quickly from the top of the 'piston'. The gas chimney can start to deform the sediment overlying it when its height equals half the depth of its base below seafloor. Deformation will be triggered in the pre-existing weaknesses that become permeable flow pathways and produce pockmarks on the seafloor which later will be merged to form the larger pockmarks or pockmark clusters with continued gas migration (Cathles et al., 2010).

According to the synthesis published by Pilcher and Argent (2007) collecting evidence from 57 published occurrences of contemporary pockmarks around the world, the most common size of pockmarks are from 10 to 250 m in diameter, the mean diameter of pockmarks is 128 m and the mean depth is 9.6 m. In the Pilcher and Argent (2007) classification pockmark greater than 1 km in diameter are coined 'mega' pockmarks. In this study area, pockmarks have wide range from most common size of 50–250 (pockmark clusters) to >1 km of 'mega' pockmark (pockmark trains).

The distribution of pockmarks in the study area shows a systematic relationship with the topography (gradient). They are mainly confined to the area with relatively high gradients in the upper part of both slopes, and they are almost absent in the lower slopes. The area of BSR occurrence broadly coincides with the distribution area of pockmarks and pipes rooting from the Pliocene channel-fan system, suggesting that gas stored underneath the BSR is the fluid responsible for the pockmarks.

5.3. Seismic expression of fluid migration

Beneath the single pockmarks, the 3D seismic data image vertical to sub-vertical cylindrical acoustic anomalies zones which are highly discontinuous or disrupted seismic reflections or depressed reflections (Fig. 13b). The vertical extent of the features ranges from c. 200 m–1200 m and they range in diameter between 300 and 400 m. Most of them have a circular shape in plan form with a depression of c. 15–30 m (Fig. 13a). The reflection amplitudes within the vertical zones are highly variable, characterized as acoustic wipe-out at depth to concave upwards low amplitude reflections occurring toward the upper part of the vertical zones, above the BSR. These concave reflections are sometimes observed locally as high amplitude reflections at the interval from BSR to seafloor. The features are stratigraphically restricted mostly to the Pliocene–Pleistocene sequences.

The geometry, scale and association of the vertical anomalies with the interpreted Pliocene fan–channel complex system suggest an interpretation of "blow-out pipes" which have been reported from a number of locations on the West Africa margins (Pilcher and Argent, 2007; Gay et al., 2007; Moss and Cartwright, 2010a; Løseth et al., 2011). High amplitude reflections within the pipes are possibly caused by velocity variations induced by cemented zones (Gay et al., 2007; Hustoft et al., 2007).

The mechanism of free gas to break through a gas-hydrate bearing formation is proposed to involve buoyancy pressure of free gas trapped underneath the hydrate zone, increasing accumulated free gas volumes until its pressure is sufficient for gas to break the seal. The complete failure of seal releases a large fraction of the accumulated gas into an upward-propagating gas chimney, which replace water like a piston as it rises (Gorman et al., 2002; Flemings et al., 2003; Cathles et al., 2010; Andresen et al., 2011). In the South African margin, the maximum thickness of gas beneath the BSR is ~300 m at a water depth of 2000 m. Any increase in column height, due to continuous gas migration below the hydrate seal, could induce failure and fracture of the BSR, with resultant gas migration through the hydrate layer (Grauls, 2001). The critical pressure at the base of the hydrate seal depends on the hydromechanical seal properties, which controls the thickness of the gas pocket beneath the BSR (Grauls, 2001). In general, the trapping potential of hydrates increases with the seafloor depth (Grauls et al., 1998). Recently, the dynamic effect of rapid sea-level change has been investigated quantitatively (Hermanrud et al., 2013), and it is possible that glacio-eustatic fluctuations during the late Quaternary would have facilitated overpressure generation and hydrofracture associated with free gas and gas-hydrate dissociation due to falling sea-level.

We suggest that buoyancy overpressure due to gas accumulation beneath hydrate-bearing near-seafloor sediments is one of the main mechanisms to generate focused fluid flow in shallow sediments in the study area. This is supported by the occurrence of focused fluid flow features, i.e., pockmarks and pipes, in the uppermost slope domains. Kilometer-scale blowout pipes suggest effective migration, and support the presence of an active petroleum system from deeper reservoirs to the surface. The abundance of pockmarks and chimneys indicates that a sufficient amount of gas has been charged into reservoirs to produce hydrofracture inducing overpressure.

6. Discussion

6.1. Gas hydrate-related BSR

The BSR extends over an area of 350 km^2 as a continuous reflection across the upper slopes of the Cameroon continental margin associated with pipes and a large scale, high amplitude Pliocene fan lobe system underneath, which suggests a large amount of free gas and gas hydrate accumulation in the shallow sediments. The BSR shows a clear cross-cutting relationship with the primary strata in the steeper upper slopes. The most striking result to emerge from the data is that strong BSRs dominate the LGS and their location is associated with the underlying Pliocene fan–channel complex system. Whereas weak BSRs are restricted to the HGS and show an association with low amplitude reflections below the BSRs. BSR amplitude variation is interpreted to be due to lithological control (porosity and permeability) on free gas migration and storage, with the better reservoir being present in the LGS sands; and limited storage capacity within the HGS muds.

The variation of BSR amplitude in the study area is consistent with earlier studies in the southeastern U.S. continental margin (Lee et al., 1994) and Blake Ridge (Holbrook et al., 1996). We identified a clear relationship with the Pliocene fan–channel complex system located underneath the BSR in the LGS. The amplitude variation indicates these channels are gas-changed.

Evidence of stored gas includes deep fluid flow features that can be mapped toward the channels and shallow focused fluid flow features (pipes and pockmarks) located above the channels. Free gas stored in the channels will create a high velocity contrast above and below, thus strengthening the BSR. Where strong BSRs abruptly turn into weak reflections, this is interpreted to be as a result of a lateral change (onlap of sandy units) to a fine-grained succession with reduced capacity to store gas beneath the BSR in the HGS.

The occurrence of free gas in the shallow sediment is also supported by a polarity reversal where high amplitude reflections crosscut the BSR (Fig. 11). When the bright reflection, interpreted as the top of a shallow sandy unit, is located beneath the BSR, the reflection is consistent with a decrease in acoustic impedance, and vice versa. This reversal of polarity is considered as a possible direct hydrocarbon indicator (DHI), similar to a bright spot or dim spot (Upadhyay, 2004). Upadhyay (2004) indicated that the replacement of brine by free hydrocarbons may result in a reversal of reflection polarity from positive to negative. If the hydrocarbons enter a thin reservoir layer, this gas-saturated layer may turn into hydrate bearing sediment when it is located within the zone of hydrate stability. The higher concentration of gas hydrate within this sediment layer may result in greater acoustic impedance (ρV) than the surrounding area, which will create a positive polarity at the top of the gas hydrate-bearing sand body (and correlatively negative polarity at the base). Below the BSR, on the other hand, the occurrence of free gas in the sediment layer will reduce the average density and decrease the acoustic impedance, hence resulting in a reversal in polarity (negative).

Further evidence for the lithological control on the presence of free gas/gas hydrate accumulation is observed in the distribution of positive high to bright amplitudes above the BSR in the GHSZ (Fig. 15). These positive high/bright spots are only observed as a part of the fan–channel complex system in the LGS. They seem to be present at the same depth and possibly within the same permeable layer that contains the high concentration of hydrate resulting in a high/bright spot. Hornbach et al. (2003) studied multichannel seismic reflection data from the Blake Ridge, and suggested that the bright spots within the GHSZ were discrete layers of concentrated hydrate formed by upward migration of free gas. The velocities within these layers are considerably higher than velocities in immediately adjacent strata (>1900 m/s).

The BSR is considered to be both a direct thermal indicator (DTI) and a direct hydrocarbon indicator (DHI) (Grauls, 2001). The BSR can be used as a DTI as gas hydrate stability occurs in a specific domain of temperature and pressure. It marks the base of the gas hydrate stability zone and therefore the BSR distribution provides direct constrain for the gas hydrate occurrence (DHI). Gas hydrate occurrence along continental margins where pressure and temperature conditions are favorable is controlled by the presence of sufficient methane in shallow sediments and their reservoir properties. Widespread occurrence of gas hydrates detected in the study area suggests that a large amount of gas has been generated in the basin. Gas may be biogenic gas and gas from the thermogenic alteration of organic matter. The conditions for methanogenic bacteria biogenic gas generation are organic matter, anoxic sulphate-free environment and at temperature less than ~75 °C (Rice and Claypool, 1981; Clayton, 1992; Pang et al., 2005). In the study area, geothermal gradient of the shallow sediment is c.5.1 °C/100 m (from Ocean Drilling Program data in lower Congo basin which have penetration depth less than 200mbsf (Wefer, 1998)). With the geothermal gradient of c.5.1 °C/100 m, the maximum depth for the biogenic gas to be generate will be 1.4 km depth. The depth of the Pliocene area is about 600 m, hence, reservoirs in that interval may be supplied by both insitu and exsitu biogenic gas and also deep thermogenic gas, the latter implied by the connection with km-long blow-out pipes and vertical stacking of amplitude anomalies I deepwater channels and fans.

Bottom simulating reflections have been reported in most West Africa margins from Nigeria to Namibia in water depths greater than 700 m (Cunningham and Lindholm, 2000; Emery et al., 1974; Hovland et al., 1997; Swart, 2009). The BSR observed in the Cameroon margin displays many characteristics that have very often been reported for the BSR related gas hydrate in the West Africa margins and elsewhere in the world. The BSRs along the Nigeria and Congo continental slopes have been reported to be the most numerous and extensive BSR areas and associated with the areas of complex structures (Cunningham and Lindholm, 2000). In this study, the extensive BSR seems to be stratigraphically controlled as it is developed above the deeply buried paleochannels at different stratigraphic levels, from the Miocene to the Pliocene (Le, 2012).

6.2. BSR anomaly – shoaling BSR within gully 3

The relationship between BSR depth and water depth in deep water generally is a near-linear function of increasing BSR depth with increasing water depth, except where focused fluid flow or anomalous geothermal conditions exist (Kvenvolden and Barnard, 1982; Minshull and Keddie, 2010). This relationship is confirmed in our data (Fig. 16a), with the only anomalous data occurring in the area of the gully (gully 3). Further analysis on the BSR within the gully was therefore undertaken. The continuous BSR within the gully was mapped (Fig. 16b, c, d). The BSRs depth below the seafloor within the gully area is shallower than the BSR in adjacent area about 43 m (Fig. 16b). Meanwhile, according to the relationship of BSR depth and water depth, the BSR depth is expected to be greater than the adjacent area as it has greater water depth. On the other hand, the BSR is also expected be pushed down (in time) due to the low velocity effect of the greater water column above gully 3. The water depth within gully 3 ranges from 1125 m to 1320 m, corresponding to BSR depth of 1280 m–1550 m, respectively. However, mapping shows that the BSR actually is in the depth range from 1190 m to 1440 m, i.e. 90–110 m shallower than the expected values for steady state conditions and a geotherm of 5.1 °C/100 m (Fig. 14).

The dynamic nature of BSRs and their equilibrium have been eloquently discussed by Hornbach et al. (2008), emphasising the roles of temperature. The BSR depth or hydrate phase boundary depth is most-likely primarily driven by temperature and to a lesser extent by pressure and salinity (Dickens and Quinby-Hunt, 1997; Sloan, 2003). An example for this is the study at Blake Ridge by Hornbach et al. (2008) based on the studies of Dickens and Quinby-Hunt (1997) and Sloan (2003), that indicates that a change of 1% salinity and 100 m in seafloor depth will only shift the BSR depth ~1.5 m and ~5 m, respectively. But a 1 °C change in thermal gradient will shift the BSR a significant 15 m. If only temperature is taken into consideration, the shallow BSR in the study area is supposed to caused by ~7 °C higher than the background temperature. The role of temperature on BSR depth became clearer when Hornbach et al. (2008) calculated the effect of erosion and sedimentation on hydrate stability. The results show an agreement with Dickens and Quinby-Hunt (1997) and Henrys et al. (2003). Deeper BSR should be expected if the ongoing sedimentation rate is faster than the conductive heat transfer, resulting in anomalous cool sediments, thus the BSR may be deeper than predicted by a steady geothermal gradient. On the other hand, the BSR would be shallower if the area is undergoing active erosion. In this case, the subsurface temperature will be higher than expected and thus result in a shallower BSR.

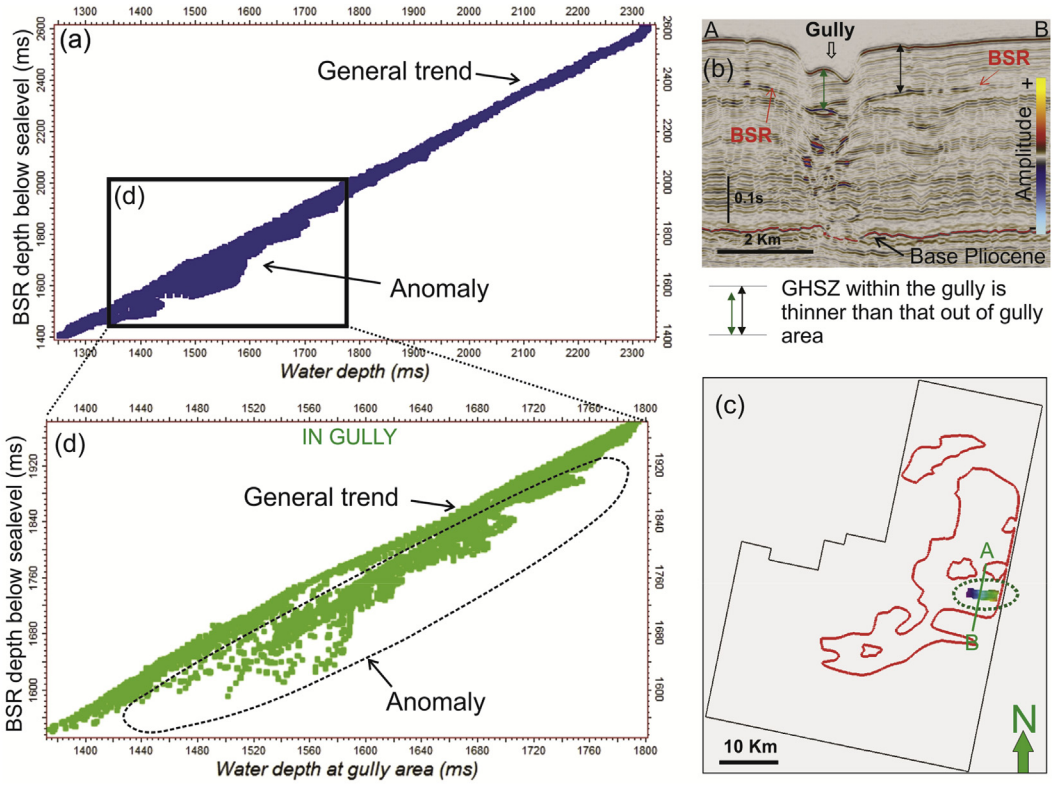

Figure 16. (a) The relationship between water depth and BSR depth (from the sea level) reveals the general trend, and the anomaly. (b) The thickness of GHSZ in the gully is thinner than outside the gully, but it is expected to be thicker due to the deeper water depth (c) Mapping of the BSR area extent and location of BSR in the gully 3. (d) Display on the graph the relationship between water depth and BSR depth for the area shown in green circle of (c). (For interpretation of the references to colour in this figure legend, the reader is referred to the web version of this article.)

Anomalous shoaling of the BSR has been documented mainly in areas of slope failure, such as in the Nankai trough (Martin et al., 2004), Storegga Slide (Berndt, 2005), Blake Ridge (Ruppel, 1997; Hornbach et al., 2008). In these areas, erosion is an obvious factor that caused shoaling. Focused advection was also considered to have a significant role in changing the depth of to the BSR. This is because fluids may be channeled through the Pliocene channel-fan system; especially vertical offset stacked channels which immediately underneath the BSR (Fig. 8 – gully 3).

Shoaling of the BSR is observed in the gully 3 which records as long term interplay of erosion and sedimentation. The gully is also characterized by the strongest BSR in any gully of the study area, suggesting a direct link with the local hydrocarbon system. The factors that control the BSR shoaling in gully 3 thus likely involve both erosion and fluid migration processes and would require further constraints from shallow coring and thermal probes to constrain further.

6.3. Conceptual model for the BSR offshore southern Cameroon

In the literature, two models of BSR formation have been proposed to explain the relationship of gas hydrates, free gas and the BSR. In the first model, gas is assumed to be generated insitu from biogenic processes from local organic material at the same depth of the GHSZ (Lee et al., 1994). In the second model, hydrates are formed by the exsolution of gas from upward moving fluids (generated by deeper thermogenic processes) as they enter the GHSZ (Hyndman and Davis, 1992).

In this study, the character, distribution and seismic evidence support for the second model or a combination of the two models with thermogenic supply dominating over in situ supply. The widespread BSR suggests the considerable amount of gas has been generated which is possibly both biogenic and thermogenic origin, and is trapped underneath a hydrate seal. The characteristics of the BSR and its relationship with other geological features such as blow-out pipes, channel systems and pockmarks have been synthesised in Figure 17. In the LGS, the presence of the strong BSR is associated with blow-out pipes, single pockmarks and high amplitude reflections below. The high amplitude reflections immediately underneath the BSR indicate the presence of free gas, trapped under the GHSZ seal, creating a high velocity contrast, thus resulting in strengthening of the BSR. In the HGS, the BSR prominently displays as a weak BSR but is also associated with the pockmark trains and pockmark clusters. The weakness of the BSR is interpreted to record less trapped free gas because of less permeable sediments and thus the resulting low velocity contrast above and below the BSR.

Bright sports (high amplitude reflections in the GHSZ) are mainly observed in the LGS which supports the notion of upward migration of gas through the Pliocene channel system and accumulation at high concentration in shallower sand bodies. The bright sports are observed close to the vertically stacked channels and thus may indicate the presence of good migration paths for gas to enter the GHSZ.

The presence of pockmarks within the gullies in the HGS is supposed to be caused by fluid venting on the seafloor. The main migration paths are possibly the channel sand associated with gullies and the accretion surfaces of sediment waves. Holbrook et al. (2002) suggested that rapid formation of large sediment waves and associated seafloor erosion in Blake Ridge during the Quaternary created high-permeability pathways for methane gas expulsion on the seafloor. The abundance of pockmark trains associated with the gullies may be further evidence of this process.

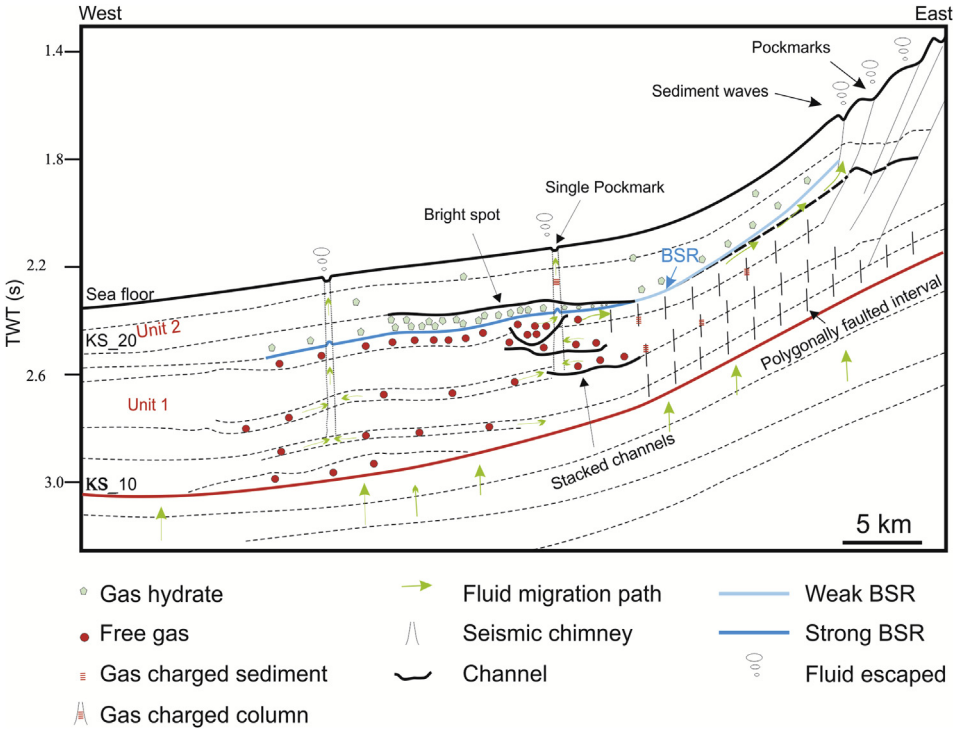

Figure 17. Schematic diagram illustrating the conceptual model for the BSR and associated features. The strength of the BSR varies from HGS to LGS which is interpreted to be the result of variation of gas hydrate and free gas concentration. Fluids migrating from the deep section are preferentially trapped in the high porosity and high permeability sediments forming high amplitude layers and interpreted to be a fan–channel complex system in the Unit 1 of the LGS. Increasing buoyancy pressure of this unit leads to vertical and upslope fluid migration, producing pipes, through the GHSZ to the seafloor, creating single pockmarks; Fluids also migrate laterally to the higher gradient of the HGS within the channel sand and are expelled to the seafloor along the boundaries of sediment waves, creating pockmark trains. The kilometre scale pipe observed is rooted at the deeper mid Miocene fan suggesting a thermogenic origin of gas which may have been supplied for the shallow sediments.

7. Conclusions

This study presents the first description of widespread free gas and gas hydrate occurrence and associated stratigraphic carriers and seal bypass systems on the Cameroon continental margin. This has been investigated in order to understand the nature of the BSR and associated subsurface fluid flow. The results add to the knowledge of understanding BSR characteristics, slope instability and also improve hazard awareness for future drilling in the region.

The main conclusions on gas hydrate-related BSR characteristics and controls on the BSR occurrence and fluid plumbing system are summarized below:

- Gas hydrate-related BSRs cover an area of at least 350 km^2 across two slopes, in water depths ranging from 940 m to 1750 m. The BSR depth below the seafloor ranges between 0.12 and 0.28 s TWT (104 m–250 m). It increases in depth with increasing water depth.
- The extensive and continuous nature of the BSR suggests a large amount of gas has migrated into the GHSZ and turned into hydrate.
- Bright spots in the hydrate stability zone are interpreted to record sediment layers containing high concentrations of gas hydrate. They coincide with the top of a Pliocene fan–channel complex. This suggests a relationship to lithology (porosity and permeability) for both migration mechanism and storage.
- The BSR strength varies significantly across two slope provinces, related to the presence of free gas trapped underneath the BSR. A strong BSR is observed in the Low-Gradient Slope (LGS), associated with the Pliocene fan–channel complex located immediately below the BSR. The BSR is weak in the High-Gradient Slope (HGS), interpreted to be due to the lack of free gas trapped below GHSZ seal. This is due to lower porosity/permeability fine grained sediments deposited in the HGS.
- Shoaling of the BSR within one (gully 3) of several seafloor gullies is associated with the presence of pockmark trains. This shoaling BSR is likely caused by a local temperature anomaly induced by advection from focused fluid supply, possibly enhanced by erosion/sedimentation effects within the gully.
- The variable morphology of seafloor pockmarks, from conical to flat-bottomed, suggests that fluid flow is still active or was active recently, possibly due to local overpressure in the pore-waters within sediments which may be caused by sufficient gas has been charged in to reservoir combining with glaico-eustatic fluctuations during Pleistocene time.

Acknowledgments

We would like to thank Sterling Energy Company for providing the 3D seismic data of the Cameroon Margin, West Africa area, and particular thanks to Martin Smith for providing number of advisory workshops during the PhD research project. We would like to thank the Vietnamese Government and the University of Manchester for financial support of this PhD research. We also would like to thank Christophe Serie for valuable discussions and the technical staff of the seismic laboratory of the University of Manchester, School of Earth, Atmospheric and Environment for the assistance during the interpretation work of this paper. We are grateful to Murphy Oil Corporation, Sterling Energy and the Cameroon Government for permission to publish this paper. We gratefully thanks the reviewers GC and PI for the time and care they have taken in reading and reviewing this paper.

References

Andresen, K.J., Huuse, M., 2011. 'Bull-eye' pockmarks and polygonal faulting in the Lower Congo Basin: relative timing and implications for fluid expulsion during shallow burial. Mar. Geol. 279 (1), 111–127.

Andresen, K.J., Huuse, M., Schodt, N.H., Clausen, L.F., Seidler, L., 2011. Hydrocarbon plumbing systems of salt minibasins offshore Angola revealed by three-dimensional seismic analysis. AAPG Bull. 95 (6), 1039–1065.

Benkhelil, J., Giresse, P., Poumot, C., Ngueutchoua, G., 2002. Lithostratigraphic, geophysical and morpho-tectonic studies of the South Cameroon shelf. Mar. Pet. Geol. 19, 499–517.

Berndt, C., 2005. Focused fluid flow in passive continental margins. Philos. Trans. R. Soc. A Math. Phys. Eng. Sci. 363, 2855.

Berndt, C., Bünz, S., Clayton, T., Mienert, J., Saunders, M., 2004. Seismic character of bottom simulating reflectors: examples from the mid-Norwegian margin. Mar. Pet. Geol. 21, 723–733.

Berndt, C., Cattaneo, A., Szuman, M., Trincardi, F., Masson, D., 2006. Sedimentary structures offshore Ortona, Adriatic Sea—deformation or sediment waves? Mar. Geol. 234, 261–270.

Binks, R., Fairhead, J., 1992. A plate tectonic setting for Mesozoic rifts of West and Central Africa. Tectonophysics 213, 141–151.

Brooks, J.M., Bryant, W.R., Bernard, B.B., Cameron, N.R., 2000. The nature of gas hydrates on the Nigerian continental slope. Ann. N. Y. Acad. Sci. 912, 76–93.

Bünz, S., Mienert, J., 2004. Acoustic imaging of gas hydrate and free gas at the Storegga Slide. J. Geophys. Res. Solid Earth. 109, B04102.

Calvès, G., Huuse, M., Schwab, A., Clift, P., 2008. Three-dimensional seismic analysis of high-amplitude anomalies in the shallow subsurface of the Northern Indus Fan: sedimentary and/or fluid origin. J. Geophys. Res. 113, B11103.

Cartwright, J., 2011. Diagenetically induced shear failure of fine-grained sediments and the development of polygonal fault systems. Mar. Pet. Geol. 28, 1593–1610.

Cartwright, J.A., Dewhurst, D.N., 1998. Layer-bound compaction faults in fine-grained sediments. Bull. Geol. Soc. Am. 110 (10), 1242–1257.

Cartwright, J.A., Lonergan, L., 1996. Volumetric contraction during the compaction of mudrocks: a mechanism for the development of regional scale polygonal fault systems. Basin Res. 8 (2), 183–193.

Cathles, L., Su, Z., Chen, D., 2010. The physics of gas chimney and pockmark formation, with implications for assessment of seafloor hazards and gas sequestration. Mar. Pet. Geol. 27, 82–91.

Clayton, C., 1992. In: Vially, R. (Ed.), Source Volumetrics of Biogenic Gas Generation, pp. 191–204.

Cunningham, R., Lindholm, R.M., 2000. Seismic evidence for widespread gas hydrate formation, offshore West Africa. In: Mello, M.R., Katz, B.J. (Eds.), AAPG Memoir 73, pp. 93–105, 93–106.

Dailly, P., 2000. Tectonic and stratigraphic development of the Rio Muni Basin, equatorial Guinea: the role of transform zones in Atlantic Basin evolution. In: Mohriak, W., Talwani, M. (Eds.), Atlantic rifts and Continental Margins. American Geophysical Union, Washington, DC, pp. 105–128.

Davison, I., 1999. Tectonics and Hydrocarbon Distribution along the Brazilian South Atlantic Margin. In: Geological Society London Special Publications 153, p. 133.

De Batist, M., Klerkx, J., Van Rensbergen, P., Vanneste, M., Poort, J., Golmshtok, A.Y., Kremlev, A.A., Khlystov, O.M., Krinitsky, P., 2002. Active hydrate destabilization in Lake Baikal, Siberia? Terra Nova 14, 436–442.

De Matos, R.M.D., 1992. The northeast Brazilian rift system. Tectonics 11 (4), 766–791.

Dickens, G.R., Quinby-Hunt, M.S., 1997. Methane hydrate stability in pore water: a simple theoretical approach for geophysical applications. J. Geophys. Res. 102, 773–783.

Dillon, W.P., Lee, M.W., Coleman, D.F., 1994. Identification of marine hydrates in situ and their distribution off the Atlantic Coast of the United States. Nat. Gas Hydrates 715, 364–380.

Emery, K.O., Uchupi, E., Phillips, J., Bowin, C., Mascle, J., 1974. The Continental Margin off Western Africa: Angola to Sierra Leone. Woods Hole Oceanographic Institution.

Flemings, P.B., Liu, X., Winters, W.J., 2003. Critical pressure and multiphase flow in Blake Ridge gas hydrates. Geology 31, 1057–1060.

Ganguly, N., Spence, G.D., Chapman, N.R., Hyndman, R.D., 2000. Heat flow variations from bottom simulating reflectors on the Cascadia margin. Mar. Geol. 164, 53–68.

Gay, A., Lopez, M., Berndt, C., Seranne, M., 2007. Geological controls on focused fluid flow associated with seafloor seeps in the Lower Congo Basin. Mar. Geol. 244, 68–92.

Gay, A., Lopez, M., Cochonat, P., Sultan, N., Cauquil, E., Brigaud, F., 2003. Sinuous Pockmark Belt as Indicator of a Shallow Buried Turbiditic Channel on the Lower Slope of the Congo Basin, West African Margin. In: Geological Society London Special Publications 216 (1), pp. 173–189.

Gee, M.J.R., Gawthorpe, R.L., Friedmann, J.S., 2005. Giant striations at the base of a submarine landslide. Mar. Geol. 214, 287–294.

Giresse, P., Aloisi, J.C., Kuete, M., Monteillet, J., Ngueutchoua, G., 1995. Quaternary sedimentary deposits on the Cameroon shelf: characterization of facies and late quaternary shorelines. Quat. Int. 29, 75–82.

Gorman, A.R., Holbrook, W.S., Hornbach, M.J., Hackwith, K.L., Lizarralde, D., Pecher, I., 2002. Migration of methane gas through the hydrate stability zone in a low-flux hydrate province. Geology 30, 327–330.

Grauls, D., 2001. Gas hydrates: importance and applications in petroleum exploration. Mar. Pet. Geol. 18, 519–523.

Grauls, D., Blanche, J., Poudre, J., 1998. Hydrate sealing efficiency from seismic AVO and hydromechanical approaches. In: Proceedings of the International Symposium on Methane Hydrates: Resources in the Near Future?, Tokyo, 20–22 October, pp. 81–86.

Henrys, S.A., Ellis, S., Uruski, C., 2003. Conductive heat flow variations from bottom-simulating reflectors on the Hikurangi margin, New Zealand. Geophys. Res. Lett. 30 (2), 4, 1065.

Hermanrud, C., Venstad, J.M., Cartwright, J., Rennan, L., Hermanrud, K., Bolås, H.M.N., 2013. Consequences of water level drops for soft sediment deformation and vertical fluid leakage. Math. Geosci. 45, 1–30.

Holbrook, W., Lizarralde, D., Pecher, I., Gorman, A., Hackwith, K., Hornbach, M., Saffer, D., 2002. Escape of methane gas through sediment waves in a large methane hydrate province. Geology 30, 467–470.

Holbrook, W.S., Hoskins, H., Wood, W.T., Stephen, R.A., Lizarralde, D., 1996. Methane hydrate and free gas on the Blake Ridge from vertical seismic profiling. Science 273, 1840–1843.

Hornbach, M.J., Holbrook, W.S., Gorman, A.R., Hackwith, K.L., Lizarralde, D., Pecher, I., 2003. Direct seismic detection of methane hydrate on the Blake Ridge. Geophysics 68, 92–100.

Hornbach, M.J., Saffer, D.M., Holbrook, W.S., Van Avendonk, H.J.A., Gorman, A.R., 2008. Three-dimensional seismic imaging of the Blake Ridge methane hydrate province: evidence for large, concentrated zones of gas hydrate and morphologically driven advection. J. Geophys. Res. 113 (B7), 15. B07101.

Hovland, M., Gallagher, J.W., Clennell, M.B., Lekvam, K., 1997. Gas hydrate and free gas volumes in marine sediments: example from the Niger Delta front. Mar. Pet. Geol. 14, 245–255.

Hustoft, S., Mienert, J., Bünz, S., Nouze, H., 2007. High-resolution 3D-seismic data indicate focussed fluid migration pathways above polygonal fault systems of the mid-Norwegian margin. Mar. Geol. 245, 89–106.

Hyndman, R.D., Davis, E.E., 1992. A mechanism for the formation of methane hydrate and seafloor bottom-simulating reflectors by vertical fluid expulsion. J. Geophys. Res. Solid Earth 97, 7025–7041.

Jobe, Z.R., Lowe, D.R., Uchytil, S.J., 2011. Two fundamentally different types of submarine canyons along the continental margin of equatorial guinea. Mar. Pet. Geol. 28 (3), 843–860.

Judd, A., Hovland, M., 2007. Seabed Fluid Flow. Cambridge University Press, New York.

Kubo, Y.S., Nakajima, T., 2002. Laboratory experiments and numerical simulation of sediment-wave formation by turbidity currents. Mar. Geol. 192, 105–121.

Kvenvolden, K.A., Barnard, L.A., 1982. Hydrates of natural gas in continental margins. Stud. Cont. Margin Geol. 631–640.

Kvenvolden, K.A., Ginsburg, G.D., Soloviev, V.A., 1993. Worldwide distribution of subaquatic gas hydrates. Geo-Marine Lett. 13, 32–40.

Le, A.N., 2012. Stratigraphic Evolution and Plumbing System in the Cameroon Margin, West Africa (PhD thesis). The University of Manchester.

Lee, M.W., Hutchinson, D.R., Agena, W.F., Dillon, W.P., Miller, J.J., Swift, B.A., 1994. Seismic character of gas hydrates on the southeastern US continental margin. Mar. Geophys. Res. 16, 163–184.

Løseth, H., Wensaas, L., Arntsen, B., Hanken, N.-M., Basire, C., Graue, K., 2011. 1000 m long gas blow-out pipes. Mar. Pet. Geol. 28, 1047–1060.

Meyers, J.B., Rosendahl, B.R., Groschelbecker, H., Austin, J.A., Rona, P.A., 1996. Deep penetrating MCS imaging of the rift-to-drift transition, offshore Douala and North Gabon basins, West Africa. Mar. Pet. Geol. 13, 791–835.

Martin, V., Henry, P., Nouze, H., Noble, M., Ashi, J., Pascal, G., 2004. Erosion and sedimentation as processes controlling the BSR-derived heat flow on the Eastern Nankai margin. Earth Planet. Sci. Lett. 222 (1), 131–144.

Minshull, T.A., Keddie, A., 2010. Measuring the geotherm with gas hydrate bottom-simulating reflectors: a novel approach using three-dimensional seismic data from the eastern Black Sea. Terra Nova 22, 131–136.

Moss, J.L., Cartwright, J., 2010a. 3D seismic expression of km-scale fluid escape pipes from offshore Namibia. Basin Res. 22 (4), 481–501.

Moss, J.L., Cartwright, J., 2010b. The spatial and temporal distribution of pipe formation, offshore Namibia. Mar. Pet. Geol. 27, 1216–1234.

Ntamak-Nida, M.J., Baudin, F., Schnyder, J., Makong, J.C., Komguem, P.B., Abolo, G.M., 2008. Depositional environments and characterisation of the organic matter of the Lower Mundeck Formation (Barremian?-Aptian) of the Kribi-Campo sub-basin (South Cameroon): Implications for petroleum exploration. J. Afr. Earth Sci. 51, 207–219.

Ntamak-Nida, M.J., Bourquin, S., Makong, J.C., Baudin, F., Mpesse, J.E., Christophe, I.N., Komguem, P.B., Abolo, G.M., 2010. Sedimentology and sequence stratigraphy from outcrops of the Kribi-Campo sub-basin: lower Mundeck Formation (Lower Cretaceous, southern Cameroon). J. Afr. Earth Sci. 58, 1–18.

Pang, X., Zhao, W., Su, A., Zhang, S., Li, M., Dang, Y., Xu, F., Zhou, R., Zhang, D., Xu, Z., 2005. Geochemistry and origin of the giant Quaternary shallow gas accumulations in the eastern Qaidam Basin, NW China. Org. Geochem. 36, 1636–1649.

Pauken, R.J., 1992. Sanaga sud field, offshore Cameroon, West Africa. In: Halbouty, M.J. (Ed.), Giant Oil and Gas Field of the Decade 1978–1988, Mobil Exploration Ventures Co Texas, AAPG Memoirs 54, pp. 217–230.

Pecher, I.A., Henrys, S.A., Wood, W.T., Kukowski, N., Crutchley, G.J., Fohrmann, M., Kilner, J., Senger, K., Gorman, A.R., Coffin, R.B., 2010. Focussed fluid flow on the Hikurangi Margin, New Zealand—evidence from possible local upwarping of the base of gas hydrate stability. Mar. geol. 272, 99–113.

Pilcher, R., Argent, J., 2007. Mega-pockmarks and linear pockmark trains on the West African continental margin. Mar. Geol. 244, 15–32.

Piper, D.J., Shor, A.N., Clarke, J.E.H., 1988. The 1929 "Grand Banks" Earthquake, Slump, and Turbidity Current. In: Geological Society of America Special Papers 229, pp. 77–92.
Rice, D.D., Claypool, G.E., 1981. Generation, accumulation, and resource potential of biogenic gas. AAPG Bull. 65, 5–25.
Ruppel, C., 1997. Anomalously cold temperatures observed at the base of the gas hydrate stability zone on the US Atlantic passive margin. Geology 25 (8), 699–702.
Serié, C., Huuse, M., Schødt, N.H., 2012. Gas hydrate pingoes: deep seafloor evidence of focused fluid flow on continental margins. Geology 5. http://dx.doi.org/10.1130/G32690.1.
Shankar, U., Riedel, M., 2010. Seismic and heat flow constraints from the gas hydrate system in the Krishna–Godavari Basin. India. Mar. Geol. 276, 1–13.
Sloan, E.D., 2003. Fundamental principles and applications of natural gas hydrates. Nature 426, 353–363.
Stow, D.A.V., Reading, H.G., Collinson, J.D., 1996. Deep seas. In: Reading, H.G. (Ed.), Sedimentary Environments, third ed. Blackwell Science, pp. 395–454.
Sultan, N., Marsset, B., Ker, S., Marsset, T., Voisset, M., Vernant, A.-M., Bayon, G., Cauquil, E., Adamy, J., Colliat, J., 2010. Hydrate dissolution as a potential mechanism for pockmark formation in the Niger delta. J. Geophys. Res. Solid Earth (1978–2012) 115.
Swart, R., 2009. Hydrate Occurrences in the Namibe Basin, Offshore Namibia. In: Geological Society London Special Publications, vol. 319 (1), pp. 73–80.
Upadhyay, S.K., 2004. Seismic Reflection Processing. Springer, Germany.
Velde, B., 1996. Compaction trends of clay-rich deep sea sediments. Mar. Geol. 133, 193–201.
Wefer, G., Berger, W.H., Richter, C., et al., 1998. Site 1076. In: Baez, L.A., Scroggs, J.M. (Eds.), Proceedings of the Ocean Drilling Program, vol. 175. Initial Reports.
Wynn, R.B., Stow, D.A., 2002. Classification and characterisation of deep-water sediment waves. Mar. Geol. 192, 7–22.